THE EPOCH OF GALAXY FORMATION

C.M. Baugh, S.Cole and C.S. Frenk

Department of Physics, Science Laboratories, South Road, Durham DH1 3LE

C.G. Lacey

Theoretical Astrophysics Center, Juliane Maries Vej 30, DK-2100 Copenhagen Ø, Denmark

To appear in ApJ., May 10 1998

ABSTRACT

We use a semi-analytic model of galaxy formation in hierarchical clustering theories to interpret recent data on galaxy formation and evolution, focussing primarily on the recently discovered population of Lyman-break galaxies at $z \simeq 3$. For a variety of cold dark matter (CDM) cosmologies we construct mock galaxy catalogues subject to identical selection criteria to those applied to the real data. We find that the expected number of Lyman-break galaxies is very sensitive to the assumed stellar initial mass function and to the normalization of the primordial power spectrum. For reasonable choices of these and other model parameters, it is possible to reproduce the observed abundance of Lyman-break galaxies in CDM models with $\Omega_0 = 1$ and with $\Omega_0 < 1$. The characteristic masses, circular velocities and star-formation rates of the model Lyman-break galaxies depend somewhat on the values of the cosmological parameters but are broadly in agreement with available data. These galaxies generally form from rare peaks at high redshift and, as a result, their spatial distribution is strongly biased, with a typical bias parameter, $b \simeq 4$, and a comoving correlation length, $r_0 \simeq 4h^{-1}$Mpc. The typical sizes of these galaxies, $\sim 0.5h^{-1}$kpc, are substantially smaller than those of present day bright galaxies. In combination with data at lower redshifts, the Lyman-break galaxies can be used to trace the cosmic star formation history. We compare theoretical predictions for this history with a compilation of recent data. The observational data match the theoretical predictions reasonably well, both for the distribution of star formation rates at various redshifts and for the integrated star formation rate as a function of redshift. Most galaxies (in our models and in the data) never experience star formation rates in excess of a few solar masses per year. Our models predict that even at $z = 5$, the integrated star formation rate is similar to that measured locally, although less than 1% of all the stars have formed prior to this redshift. The weak dependence of the predicted star formation histories on cosmological parameters allows us to propose a fairly general interpretation of the significance of the Lyman-break galaxies as the first galaxy-sized objects that experience significant amounts of star formation. These galaxies mark the onset of the epoch of galaxy formation that continues into the present day. The basic ingredients of a consistent picture of galaxy formation may well be now in place.

Subject headings: galaxies: evolution - galaxies:formation - galaxies:fundamental parameters

1. INTRODUCTION

Observational studies of galaxy formation and evolution have progressed at a breathtaking pace over the past couple of years. Data from the refurbished Hubble Space Telescope, the Keck and other large telescopes are now providing quantitative information on essential properties of the galaxy population – number densities, luminosities, colours, morphologies and star formation rates – over a large span of cosmic time. These data are beginning to sketch out an empirical picture of galaxy formation and evolution from redshift $z \simeq 4$ to the present.

Evolution has now been established and quantified in: *(i)* the neutral hydrogen and metal content of the universe since $z \simeq 4$ (Lanzetta, Wolfe & Turnshek 1995, Storrie-Lombardi et al. 1996, Wolfe et al. 1995, Lu et al. 1996); *(ii)* the galaxy luminosity function since $z \simeq 1$ (Lilly et al. 1995; Ellis et al. 1996); *(iii)* the morphology of field and cluster galaxies since $z \simeq 0.8$ (e.g. Abraham et al. 1996, Dressler et al. 1994, Smail et al. 1997). The most recent addition to this remarkable list of observational advances is the discovery of a large population of *actively star-forming galaxies at $z \simeq 3$*, identified by their redshifted Lyman con-

tinuum breaks (Steidel et al. 1996a, hereafter S96). It is this population that we are primarily concerned with in this paper.

One of the earliest windows on the physical processes at play in galaxy formation is provided by studies of primordial gas clouds detected in absorption against background quasars. The comoving density of neutral hydrogen present in damped Lyman-alpha clouds peaks at $z \simeq 3$ when it was comparable to the mass in baryons seen in galactic disks today (Storrie-Lombardi et al. 1996). The decline in the abundance of neutral hydrogen clouds seems to be accompanied by a gradual build-up of their metal content (Lu et al. 1996). A population of bright galaxies is certainly well established by $z = 1$ (Lilly et al. 1995, Ellis et al. 1996, Kauffmann, Charlot & White 1996). In the CFRS survey of Lilly et al. , evolution is manifest in a systematic variation of the shape of the luminosity function of blue galaxies and a brightening of their characteristic luminosity with increasing lookback time. The luminosity function of red galaxies, on the other hand, seems to have changed little over this redshift interval, although the fraction of galaxies that have the colours of passively evolving

ellipticals appears to fall to one third of its present day value by $z = 1$ (Kauffmann et al. 1996).

On the whole, galaxies appear to be smaller and increasingly irregular at higher redshift (Driver et al. 1995, Glazebrook et al. 1995a, Abraham et al. 1996, Smail et al. 1996, Odewahn et al. 1996, Pascarelle et al. 1996, Lowenthal et al. 1997.) For example, the class of "irregular/merger" galaxies which are relatively rare at bright magnitudes makes up about a third to a half of all galaxies with $I_{AB} \simeq 25$. The median redshift at this apparent magnitude (the faintest at which automated morphological classification is possible on high resolution HST images) is $z \simeq 0.8$. Similarly, the fraction of spirals in rich clusters at $z \simeq 0.5$ is higher than in present day clusters (Dressler et al. 1994). All these studies leave little doubt that the galaxy population has evolved significantly since $z = 1$.

The discovery of a large population of Lyman-break galaxies at $z > 3$ provides the first opportunity for statistical studies of evolutionary processes in galaxies beyond $z = 1$. Steidel and collaborators (Steidel & Hamilton 1992, 1993; Steidel, Pettini & Hamilton 1995; S96) searched for high redshift galaxies by selecting objects in a colour-colour plane constructed from images in customised U_n, G and $\mathcal{R}$ band filters. For galaxies in the redshift range $3.0 < z < 3.5$, the Lyman limit discontinuity passes through the U_n filter. Opacity due to intervening neutral hydrogen increases the strength of the Lyman discontinuity regardless of the shape of the intrinsic spectral energy distribution of the galaxy (Madau 1995). Thus, a galaxy in this redshift range will be faint in the U_n band (thus becoming a "UV-dropout") and so will have a very red $U_n - G$ colour, whilst possibly having a blue $G - \mathcal{R}$ colour if it is undergoing significant star formation. A similar strategy has been successfully implemented in the Hubble Deep Field (HDF) by Steidel et al. (1996b) and Madau et al. (1996). The HST U filter has a shorter median wavelength than the U_n filter of the ground-based observations, and so colour selected objects in the HDF span a wider range of redshifts from $2 \lesssim z \lesssim 4.5$.

Follow-up spectroscopy of the UV drop-out candidates by S96 on the Keck telecope confirmed that these galaxies lie mostly in the expected redshift range, $3.0 \leq z < 3.5$. Their spectra resemble those of nearby starburst galaxies. From the apparent $\mathcal{R}$-band magnitude, a dust-free model for the spectral energy distribution in the UV, and an assumption about the initial stellar mass function (IMF), S96 inferred star formation rates in these galaxies in the range $1 - 6h^{-2}\mathrm{M_\odot yr^{-1}}$ for a critical density universe, where we have expressed Hubble's constant as $H_0 = 100h\,\mathrm{km\,s^{-1}Mpc^{-1}}$. Similarly low star formation rates have been inferred by Lowenthal et al. (1997) for 11 galaxies in the HDF at $z = 2 - 4.5$. From the width of saturated interstellar absorption lines, S96 inferred tentative one-dimensional velocity dispersions in the range $\sigma_{1D} = 180 - 320\mathrm{km\,s^{-1}}$. They concluded that the Lyman-break galaxies they discovered could be the progenitors of the spheroidal components of present day galaxies.

The current state of empirical knowledge on galaxy formation has been nicely summarized by Madau et al. (1996) and Madau (1996) in the form of a "cosmic star formation history." Combining a variety of surveys (including the CFRS and the Lyman-break galaxy surveys),

they derived metal production and star formation rates as a function of redshift, from $z = 0$ to $z \simeq 5$. Observed star formation rates over this redshift range are typically a few solar masses per year for individual galaxies. The integrated star formation rate never differs by more than an order of magnitude over this entire redshift range, although a peak of activity seems to have occured at $z \simeq 1$. The total amount of metals produced by the observed populations is comparable to the amount of metals seen in massive galaxies today, suggesting that the bulk of the cosmic star formation has now been identified.

In this paper we employ the semi-analytic model developed in a series of earlier papers (Cole et al. 1994; Heyl et al. 1995; Baugh et al. 1996a, 1996b), to investigate the significance of the Lyman-break galaxy population within the context of hierarchical clustering theories of galaxy formation. We consider the circumstances under which such a population may form and we focus on the connection between these high redshift objects and galaxies seen in various evolutionary stages at lower redshifts. We use the available data to test in detail our earlier theoretical predictions for the way in which galaxies are built up from small fluctuations in a universe dominated by cold dark matter (CDM). Specifically, we test the prediction of White & Frenk (1991), Lacey et al. (1993) and Cole et al. (1994) that the bulk of the stars present in galaxies today formed relatively recently, with a median redshift of star formation of only $z \simeq 1$. The results of these comparisons are very encouraging and suggest a general picture of galaxy formation and evolution which is consistent with the expectations from a broad class of hierarchical clustering cosmologies.

A more basic attempt to investigate whether the abundance of S96 Lyman-break galaxies is consistent with cold dark matter models was recently carried out by Mo & Fukugita (1996). They used the Press & Schechter (1974) formalism to calculate the number density of halos with velocity dispersion in excess of $\sigma_{1D} = 180\mathrm{km\,s^{-1}}$, making simple assumptions about the time required for a galaxy to form in each halo. They concluded that a range of low-density COBE-normalized CDM models are compatible with the data.

Our semi-analytic galaxy formation scheme is briefly reviewed in Section 2, where we discuss our procedure for generating mock catalogues of high redshift galaxies. The colour selection criteria of S96 are reviewed in Section 3.1 and the abundance of galaxies that meet these constraints in a variety of cosmological models is given in Section 3.2. The expected properties of high redshift galaxies – masses, star formation rates, sizes, clustering, etc – are presented in Section 3.3. Our models predict the entire evolutionary history of galaxies and so, in Section 4, we illustrate the eventual fate of a few high redshift examples and examine the statistical properties of the descendants of the Lyman-break objects. In Section 5, we recast the Cole et al. (1994) predictions for the cosmic star formation history in a manner that is directly comparable to the Madau et al. (1996) data, and we also compare our predicted evolution in the neutral gas fraction with observations. Finally, we present our conclusions in Section 6.

2. SEMI-ANALYTIC MODELLING OF GALAXY FORMATION

2.1. *General description of the model*

Semi-analytic modelling is a novel technique for calculating *ab initio* the evolutionary properties of galaxies in cosmological models in which structure forms hierarchically. The growth of dark matter halos by accretion and mergers is followed statistically, while physically motivated rules are used to describe the cooling of gas in these halos, the transformation of cold gas into stars, and the effects of feedback from massive stars on the dynamics of the gas. The spectrophotometric properties of the stars that form are calculated from a spectral synthesis model. The basic physical concepts, mathematical formalisms, and first applications of semi-analytic modelling are presented in White & Rees (1978), Cole (1991), Lacey & Silk (1991), White & Frenk (1991), Kauffmann, White & Guiderdoni (1993), and Cole *et al.* (1994). The technique has now been successfully applied to a variety of problems in galaxy formation (Lacey et al. 1993; Kauffmann, Guiderdoni & White 1994; Heyl et al. 1995; Kauffmann 1995, 1996a,b and Baugh et al. 1996a,b, Frenk et al. 1996, 1997).

The basic rules that govern the physical processes in the galaxy formation scheme adopted in this paper are presented in detail in Cole *et al.* (1994). In brief, when a dark matter halo collapses, its associated gas is assumed to be shock-heated and to settle into quasistatic equilibrium at the virial temperature of the halo. This gas cools radiatively over the lifetime of the halo and cold gas is turned into stars at a rate proportional to the instantaneous cold gas mass. Feedback from supernovae and stellar winds returns some of the cold gas to the hot phase, strongly inhibiting star formation in low circular velocity halos. During a merger, the dark matter halos coalesce, but the galaxies within them can survive longer, eventually merging on a timescale related to the dynamical friction time.

For this analysis, we have upgraded the Cole et al. (1994) model in various ways. The main modification is the replacement of the "block model" (Cole & Kaiser 1988) as the description of the merger history of dark matter halos. In the new scheme we use a Monte Carlo method based on the analytical expression for the halo progenitor mass function derived from the "extended Press-Schechter theory" (Bond et al. 1991; Bower 1991; see also Lacey & Cole 1993) to generate binary merger trees. Each tree describes a possible merger history for a halo of specified final mass. At each branch in the tree a halo splits into two progenitors, but unlike in the "block model," the mass ratio of the two progenitors can take any value. This technique enables the merger process to be followed with high time resolution, as timesteps are not imposed on the tree but rather are controlled directly by the frequency of mergers. It is similar in spirit to the method used by Kauffmann et al. (1993), but has several advantages, including that it does not require the storage of large tables of progenitor distributions. The new merger scheme is fully described in Lacey & Cole (in preparation).

A further modification to the scheme is that the singular isothermal sphere model adopted by Cole et al. as a description of the dark matter halo density profile has been replaced by the analytical form proposed by Navarro, Frenk & White (1996) on the basis of high resolution N-body simulations. In the original Cole et al. model all the gas that could cool over the entire life of the halo was assumed to be available to form stars from the beginning of the halo lifetime. We now estimate the supply of cold gas available to form stars by calculating the cooling rate at a series of discrete timesteps in which successive shells of gas can cool.

In our scheme, a cosmological model is specified by an assumption about the nature of the dark matter together with values for the cosmological parameters: the mean cosmic density (Ω_0), the cosmological constant (Λ_0), Hubble's constant ($H_0 = 100h\mathrm{kms}^{-1}\mathrm{Mpc}^{-1}$), the rms mass fluctuations in spheres of radius $8h^{-1}\mathrm{Mpc}$ (σ_8), and the mean baryon density in units of the critical density (Ω_b). Our galaxy formation prescription requires specifying 6 physical parameters: (i) a star formation timescale ($\tau_0^\star$), (ii) a "feedback parameter," (iii) the shape of the initial mass function (IMF) of stars, (iv) an overall luminosity normalisation given by the ratio of the total mass in stars, including brown dwarfs, to the mass in luminous stars, (v) a merger timescale for galaxies, and (vi) the threshold mass for a galaxy merger to turn a disk into a spheroid (see Cole et al. 1994 and Baugh et al. 1996b for further details.)

The general strategy that we have adopted in this and previous papers (Baugh et al. 1996ab, Frenk et al. 1996, 1997), is to fix the first 5 basic parameters of the model to obtain the best possible match to the local B-band and K-band galaxy luminosity functions and the sixth parameter to reproduce the local relative abundances of ellipticals, S0's and spirals. It turns out that these requirements severely restrict the allowed range of parameter values, except for the IMF which in any of the commonly used forms (ie. Salpeter (1955), Miller-Scalo (1979) or Scalo (1986)) has little effect on the predicted *local* luminosity function. The evolution of the characteristic luminosity, L_*, however, is sensitive to the choice of IMF, which therefore affects predictions for the counts of faint galaxies (see Cole et al. 1994). For the most part, we have adopted the same values of the parameters as used in the fiducial model of Cole et al., allowing ourselves the freedom to use different forms for the IMF. We again assume that feedback is a strong function of the halo circular velocity. The two exceptions are that we have slightly reduced the star formation timescale, $\tau_0^\star$, from 2 to 1.5 Gyr and we have doubled the ratio of the galaxy merger timescale to the dynamical time in the halo. The former change leads to an abundance of Lyman-break galaxies in better agreement with the data (c.f. § 3.2) while the latter change compensates for minor differences introduced by our new Monte-Carlo scheme for the halo merger trees. With this choice of parameters, our new model produces luminosity functions that are very similar to those published by Cole et al. We have updated the original Bruzual-Charlot stellar population synthesis model with their new version (also for solar metallicity only; Bruzual & Charlot 1993, Charlot, Worthey & Bressan 1996.)

Fixing the model parameters by reference to a small subset of the data produces a fully specified model which can then be tested against other data, particularly high redshift data. Thus specified, our model has predictive power and we have presented a number of specific predictions in

earlier papers. Two of these are particularly relevant to the present discussion. The first concerns the redshift distribution of a survey of faint galaxies limited to magnitude $B = 24$ (see figure 20 of Cole et al. 1994). Data have now been obtained by Glazebrook et al. (1995b) and by Cowie et al. (1996). Our model predictions are in good agreement with these data, as may be seen in Fig. 1 of Frenk et al. (1997) (see also Fig. 15 of White & Frenk 1991 and Kauffmann, Guiderdoni & White 1994). The second prediction to which we will return in Section 5 of this paper, is the cosmic star formation history, presented in Figure 21 of Cole et al. (1994) and in Fig. 14 below.

2.2. *Modelling galaxies at high redshift*

We begin by constructing merger trees for a grid of halo masses, specified at some redshift z_{halo}. Typically, we generate between 5 and 20 different realizations for each mass, depending upon the Press-Schechter abundance. The galaxy formation rules are applied along the branches of each halo tree, starting at the highest redshift of interest and propagating through to z_{halo}. Volume-limited samples or redshift catalogues are generated from the model output by weighting the galaxies in a halo tree of a given mass by its predicted Press-Schechter abundance at z_{halo}. Mock catalogues consisting of galaxies selected according to any colour-magnitude criteria can be readily generated from the model output.

To construct mock catalogues with the selection criteria of S96, we calculate broad band colours for the model stellar populations using the same set of customised filters employed by S96. (The filter functions were kindly provided by C. Steidel.) The dominant effect that determines whether a galaxy is a UV dropout is absorption of the galactic UV light by intervening cold gas. We calculate the effect of absorption on the spectral energy distributions (SEDs) of high redshift galaxies using the procedure developed by Madau (1995). In this way, we are able to select model galaxies according to exactly the same colour criteria as applied to the observational data by S96.

For most of this study we have generated trees starting at $z_{halo} = 2.6$. A high starting redshift is desirable in order to minimize inaccuracies at the high mass end of the mass distribution of progenitors introduced when the Monte-Carlo scheme is applied over a large range of expansion factor (Lacey & Cole, in preparation). We have checked, however, that our results are insensitive to the exact choice of z_{halo}. To obtain the expected total number of galaxies in the apparent magnitude range observed by Steidel et al., $\mathcal{R}_{AB} < 25.0$, we also generated mock galaxy samples from a grid of halo masses laid down at $z_{halo} = 0$. At $\mathcal{R}_{AB} < 25.0$, the median redshift is $z \sim 0.7$.

3. MODEL RESULTS

In this section we investigate the properties of the Lyman-break galaxies that form in our models and, wherever possible, we compare these to the properties of the real Lyman-break galaxies discovered by S96. Specifically, we consider the number density, masses, star formation rates and sizes of these galaxies and we present predictions for their clustering properties. To fully specify a model we need to adopt values for the cosmological parameters, Ω_0,

Λ_0, h and σ_8, and also a value for the baryon fraction, Ω_b, and an IMF. There are considerable uncertainties in these choices. We carry out calculations in three different cosmological models: the standard CDM model ($\Omega_0 = 1$, $h = 0.5$, $\sigma_8 = 0.67$); a flat, low-density CDM model ($\Omega_0 = 0.3$, $\Lambda_0 = 0.7$, $h = 0.6$, $\sigma_8 = 0.97$) and an open CDM model ($\Omega_0 = 0.4$, $h = 0.6$, $\sigma_8 = 0.68$). These parameters are typical of those favoured by large-scale structure constraints. For example, all of our models produce approximately the correct abundance of galaxy clusters at the present day and, under standard assumptions, the low-density models also match the 4-year COBE microwave background anisotropy data (Bennet et al. 1996; Liddle et al. 1996; White, Efstathiou & Frenk 1993; Eke, Cole & Frenk 1996; Viana & Liddle 1996; Cole et al. 1997.) For our standard $\Omega_0 = 1$ cosmology, we vary the normalisation of the primordial fluctuation spectrum, considering both the above value, $\sigma_8 = 0.67$, adopted in the fiducial model of Cole et al. (1994), and the lower value, $\sigma_8 = 0.5$, preferred by Eke, Cole & Frenk (1996) for consistency with the observed cluster X-ray temperature function.

We consider models with two different baryon fractions, $\Omega_b h^2 = 0.015$ and $\Omega_b h^2 = 0.030$. The first agrees with the estimate by Copi, Schramm & Turner (1996) from Big Bang nucleosynthesis and the second is consistent with the claim of Tytler, Fan & Burles (1996) of a low primordial deuterium abundance in gas clouds at high redshift. We consider three possibilities for the IMF, all of which are consistent with solar neighbourhood data, given the uncertainties in its past star formation history: Miller-Scalo (1979), Scalo (1986) and Salpeter (1955) (see figure 4 in Cole et al. 1994 for the specific parametrizations used). The parameters of these models (and of variants considered below) are summarized in Table 1.

3.1. *Two-colour selection*

We first consider the broad-band colours of our model galaxies and test the assumption that high redshift galaxies can be efficiently identified from their location in the $U_n - G$ vs $G - \mathcal{R}$ colour-colour plot constructed by S96. The analysis of Steidel, Hamilton & Pettini (1995) suggests that galaxies with redshifts in the range $3.0 < z < 3.5$ should lie within the trapezium bounded by the dashed lines in Fig. 1. At these redshifts, the Lyman break passes through the observer's frame U_n band.

Our predicted colour-colour diagram, for the case of standard CDM, is shown in Fig. 1a. The data plotted correspond to an area of 14.6 square arcminutes, equal to the area of the Q0347-3819 field observed by Steidel, Pettini & Hamilton (1995). (For clarity the points have been given small random displacements in the x and y directions. The localizations of the points in bands reflect the discrete set of output redshifts.) The open triangles in Fig. 1a indicate galaxies that have redshifts in the range $3.0 < z < 3.5$. As anticipated by Steidel et al. (1995), all galaxies with $3.0 < z < 3.5$ lie inside the trapezium in Fig. 1a. However, our models show some contamination by galaxies with redshifts in the range $2.7 < z < 3.0$ that congregate near the bottom-left corner of the trapezium. This contamination is, in fact, consistent with the evolutionary tracks shown in figure 2 of Steidel et al. (1995).

Arbitrarily deep Lyman breaks cannot be measured in
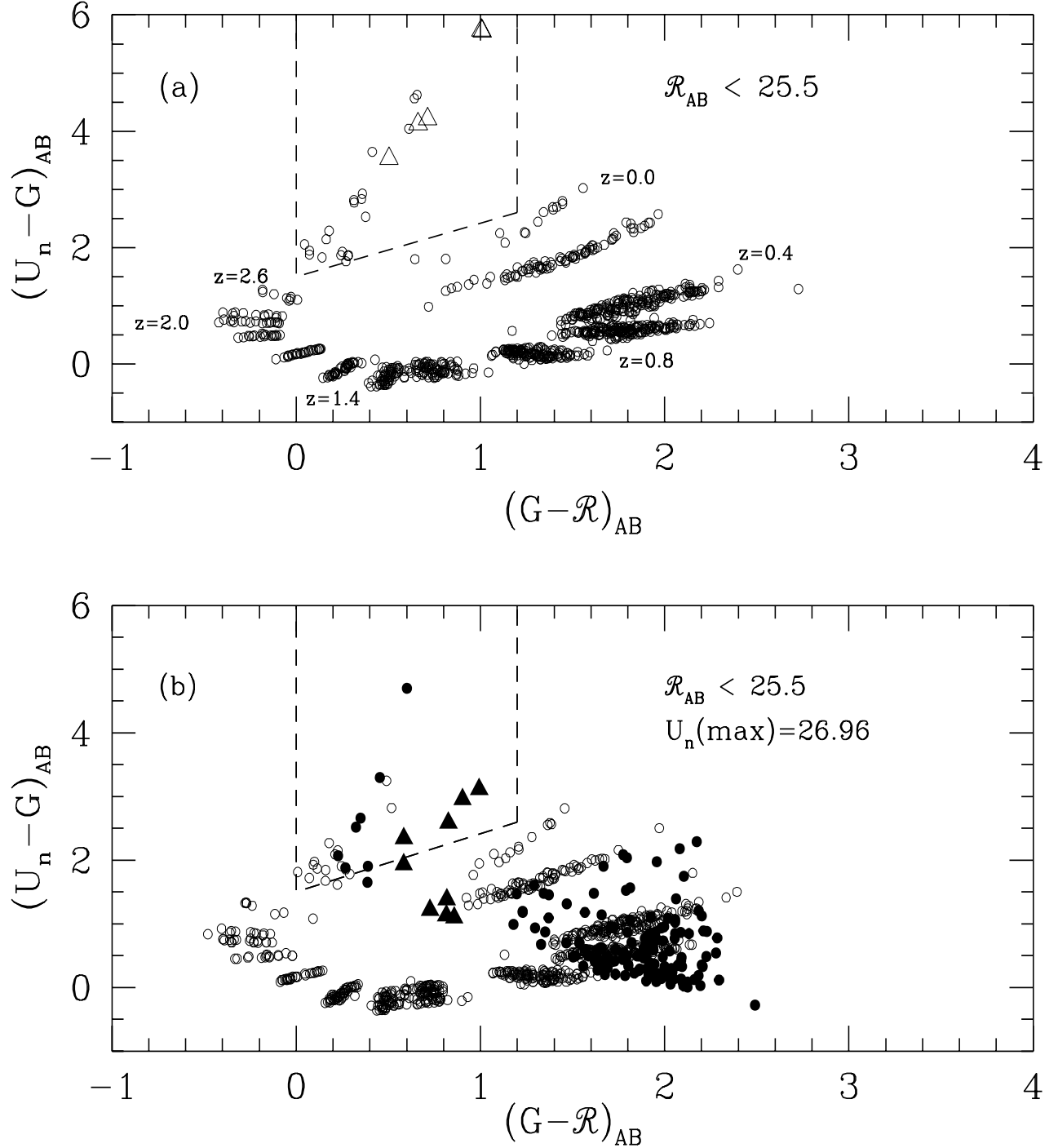
FIG. 1 Colour-colour diagrams for galaxies in the standard CDM model. Galaxies brighter than $\mathcal{R}_{AB} = 25.5$ are plotted; the area of the mock field sampled is 14.6 square arcminutes. (a) $U_n - G$ colours computed from the true U_n magnitude for all galaxies. The open circles show galaxies with redshifts $z < 3.0$ and the open triangles galaxies with redshifts in the range $3.0 < z < 3.5$. Model results are output at specific redshifts and this is reflected in the discrete regions populated in the diagram. The redshifts of selected outputs are indicated. (b) $U_n - G$ colours computed by setting the U_n magnitude to a detection limit of $U_n = 26.96$ whenever U_n is fainter than the detection limit. Galaxies in this class are denoted by filled symbols. As in panel (a), the triangles denote galaxies with redshifts in the range $3.0 < z < 3.5$.

practice because the observations are subject to a detection limit in the U_n band. For the Q0347-3819 field, the 3σ detection limit is $U_n = 26.96$. Fig. 1b illustrates the effect of imposing such a detection limit on the appearance of the colour-colour plot. Whenever a galaxy has a true U_n magnitude fainter than the field limit, we plot it at the assumed U_n limit using a filled symbol. A significant fraction of high redshift galaxies now lie below the trapezium region, confirming the remark by Steidel et al. (1995) that their selection of candidates is likely to be an underestimate of the true abundance.

Comparison of Fig. 1b with figures 4, 7, 10 and 13 of Steidel et al. (1995) shows that our models tend to produce too few galaxies with $(U_n - G)$ and $(G - \mathcal{R})$ less than unity. Galaxies in this part of the observational diagram are likely to be predominantly faint foreground dwarf irregulars. The discrepancy may be due in part to our use of solar metallicity stellar populations. This is also apparent in the comparison between our models and the local luminosity function determined by Lilly et al. (1995) from the CFRS survey (See figure 16 of Baugh, Cole & Frenk 1996b.) Beyond $z \gtrsim 0.2$, however, the luminosity functions of our models for both red and blue galaxies agree reasonably well with the CFRS data.
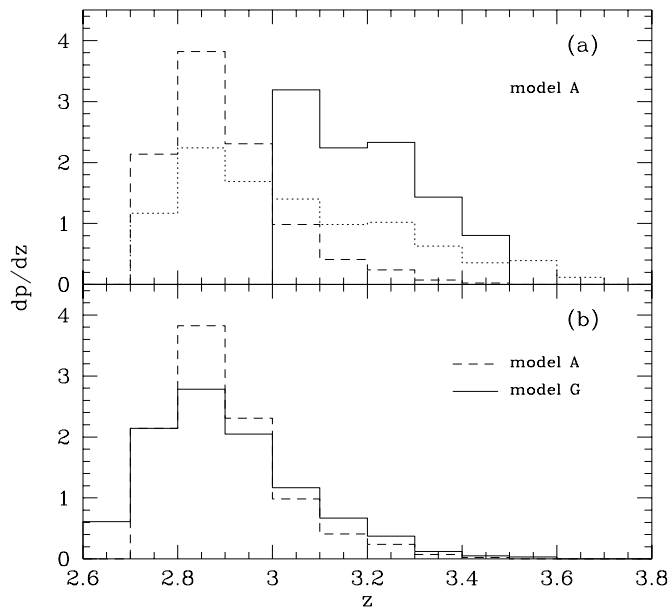
FIG. 2 Predicted redshift distributions for galaxies brighter than apparent magnitude $\mathcal{R}_{AB} = 25.0$ selected in various ways. Panel (a) shows results for our standard CDM model A. The solid line shows the distribution for galaxies with redshift in the range $3.0 < z < 3.5$. The dotted line shows the distribution for galaxies that meet the colour criteria of Steidel et al. (1995). The dashed line refers to galaxies that meet the Steidel et al. (1995) colour selection, after the detection limit in U_n for a typical observed field has been applied - model galaxies fainter than this in U_n are assigned this limiting magnitude. In panel (b) the dashed histogram is repeated from panel (a) and the solid histogram shows the corresponding redshift distribution of galaxies brighter than $\mathcal{R}_{AB} = 25$ in the low-Ω model G brighter than $\mathcal{R}_{AB} = 25$ that satisfy the Steidel et al. colour selection criteria, taking into account the typical field limit in U_n. These and subsequent histograms are normalized so that

they enclose unit area.

3.2. *The Abundance of high redshift galaxies*

Steidel, Hamilton & Pettini (1995) defined a "robust candidate" for a Lyman-break galaxy in the redshift range $3.0 < z < 3.5$ to be an object brighter than $\mathcal{R}_{AB} = 25$, with $U_n - G$ and $G - \mathcal{R}$ colours in the trapezium region of Fig. 1 and which is undetected in the U_n band. They estimated the surface density of robust candidates to be $0.40 \pm 0.07 \text{arcmin}^{-2}$, corresponding to 1.3% of their total counts brighter than $\mathcal{R}_{AB} = 25$. These counts are 30 arcmin^{-2}, with a Poisson uncertainty of 2%. Brainerd et al. (1995) quote a value of 47 arcmin^{-2} for the counts to the same magnitude. The difference seems to stem from different incompleteness corrections and uncertainties in the conversion from aperture to total magnitudes.

We now examine which, if any, of our hierarchical clustering models produces an acceptable abundance of Lyman-break galaxies. The parameters of the models we have investigated are summarized in columns 2-6 of Table 1. The seventh column gives the luminosity normalization of each model, Υ, which is defined as the ratio of the total mass in stars formed in the model to the mass formed in luminous stars *i.e.* stars with mass greater than $0.1 M_\odot$. This parameter is set in all cases to match the knee of the observed local field galaxy luminosity function, as described by Cole et al. (1994).

Table 2 gives the abundance of galaxies predicted by our models. Where available the observed values are shown in the bottom row of the table. The second column, $\mathcal{N}(R_{AB} < 25.0)$, gives the total number of galaxies brighter than $\mathcal{R}_{AB} = 25$. The next three columns demonstrate the effect of applying various selection criteria to this $\mathcal{R}_{AB} < 25$ sample. The third column, $\mathcal{N}(3.0 < z < 3.5)$, gives the number of galaxies per square degree with redshift in the range $3.0 < z < 3.5$. The fourth column, $\mathcal{N}(\text{colour})$, gives the number of galaxies in the region of the colour-colour diagram from which Steidel et al. (1995) selected their high redshift candidates. As shown in Fig. 1, a significant fraction of these galaxies are at redshifts just below 3. The fifth column, $\mathcal{N}(\text{colour} + U_n)$, is the number of galaxies remaining in the colour selected region after the $U_n \leq 26.96$ magnitude limit for the Q0347-3819 field is applied and model galaxies fainter than this have had a 3σ lower limit assigned for their $U_n - G$ colour. This removes roughly half of the high redshift candidates in column 4 from the colour selected region. The final column gives the fraction of galaxies that meet the colour selection criteria, after applying a typical field limit in U_n, as a percentage of the total counts brighter than $\mathcal{R}_{AB} = 25.0$

It is clear from Table 2 that the abundance of high redshift galaxies expected in a given cosmology is very sensitive to the adopted IMF and to σ_8, the normalisation of the primordial power spectrum. For example, replacing the Scalo by the Miller-Scalo IMF in our fiducial standard CDM model, produces an increase of nearly a factor of 20 in the number of high redshift galaxies listed in column 5. This sensitivity arises because, when normalized to the same total mass in luminous stars, the Miller-Scalo IMF contains several times more stars of around $10 M_\odot$ than the Scalo IMF. Similarly, increasing σ_8 in the $\Omega_0 = 1$ model from 0.5 to 0.67 increases the number of high red-
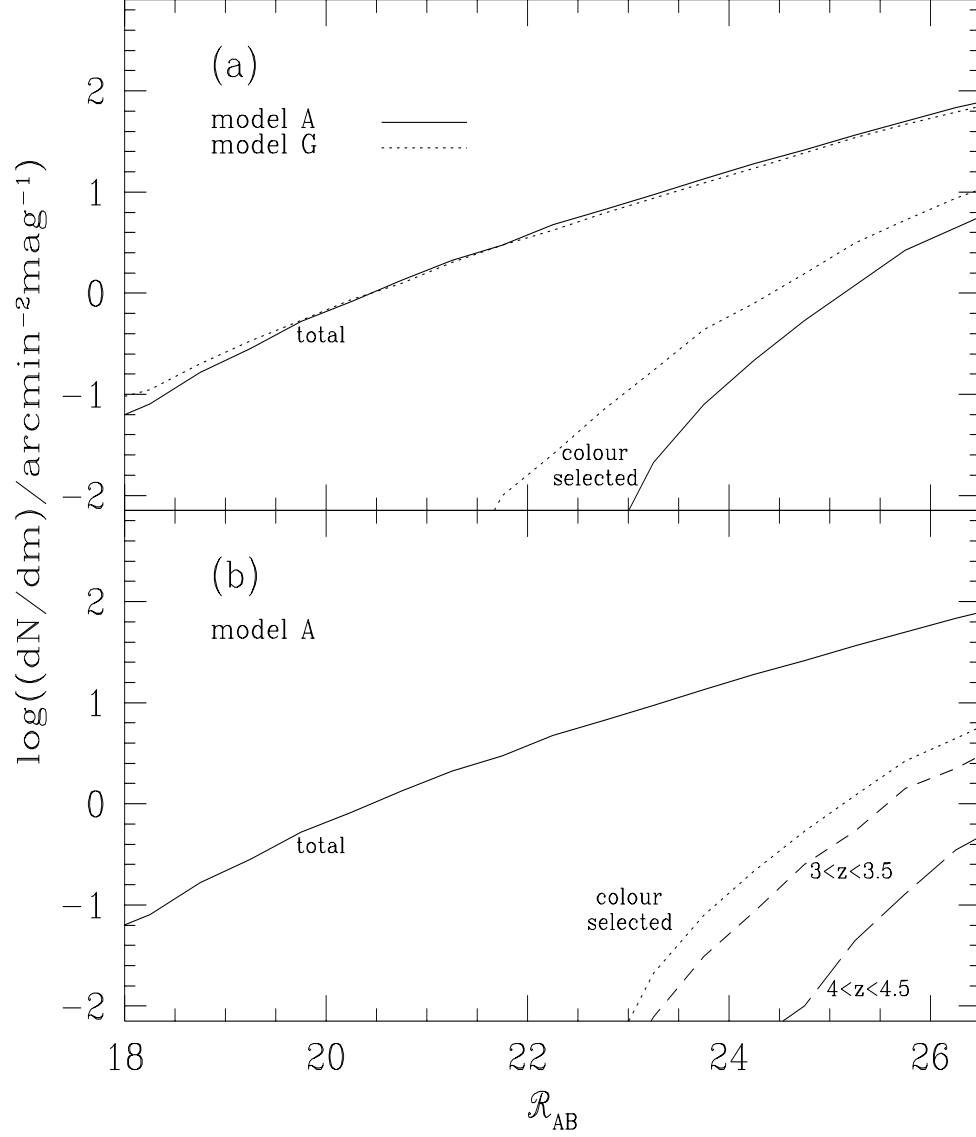
FIG. 3 Predicted galaxy number counts. In panel (a), the higher amplitude pair of lines shows the total counts in model A (solid line) and model G (dotted line). The lower amplitude pair of lines shows the counts of galaxies in each of these models that satisfy the Steidel et al. colour selection criteria alone, without any constraint on their U_n magnitudes. In panel (b) the total counts in model A are again shown by the solid line. The dotted line now shows the counts of colour selected galaxies; the short dashed line shows the counts of galaxies with redshifts in the range $3.0 < z < 3.5$; and the long-dashed line shows the counts of galaxies with redshifts in the range $4.0 < z < 4.5$.

TABLE 1

Model parameters. Columns 2-6 give the values of the cosmological parameters defined in the text. Column 7 gives, Υ, the ratio of the total mass in stars to the mass in luminous stars. Column 8 indicates the stellar initial mass function (IMF) used.

model	Ω_0	Λ_0	h	σ_8	Ω_b	Υ	IMF
A	1.0	0.0	0.5	0.67	0.06	2.8	Miller-Scalo
B	1.0	0.0	0.5	0.67	0.06	2.3	Scalo
C	1.0	0.0	0.5	0.67	0.06	1.5	Salpeter
D	1.0	0.0	0.5	0.50	0.06	2.5	Miller-Scalo
E	1.0	0.0	0.5	0.67	0.12	6.4	Miller-Scalo
F	0.4	0.0	0.6	0.68	0.04	2.8	Miller-Scalo
G	0.3	0.7	0.6	0.97	0.04	2.4	Miller-Scalo
H	0.3	0.7	0.6	0.97	0.08	4.2	Miller-Scalo

TABLE 2

The abundance of high redshift galaxies per square degree brighter than $\mathcal{R}_{AB} = 25$ for the models listed in Table 1. The quoted numbers are derived from 10 realisations of a catalogue each covering 0.1 square degrees. The final row gives results from the observational study of S96

model	$\mathcal{N}(R_{AB} < 25.0)$	$\mathcal{N}(3.0 < z < 3.5)$	$\mathcal{N}(\text{colour})$	$\mathcal{N}(\text{colour} + U_n)$	% of $\mathcal{N}(\mathcal{R}_{AB} < 25.0)$
A	153 000	890	2000	1000	0.7
B	108 000	50	130	60	0.05
C	142 000	1100	2400	1300	0.9
D	117 000	60	180	110	0.09
E	152 000	1100	2100	1100	0.7
F	101 000	1100	2200	1000	1.0
G	126 000	2400	5100	2900	2.3
H	158 000	4200	8500	4700	3.0
observed	110 000	–	–	1400 ± 300	1.3 ± 0.3

shift galaxies by a factor of 10. This dependency reflects the fact that the brightest Lyman-break galaxies at $z \simeq 3$ tend to come from the tail of rare objects in the mass distribution at this redshift. With our procedure for normalizing the luminosity of the models, the predicted abundances are insensitive to the value of Ω_b. However, the precise value of Υ does affect the abundances; reducing Υ (at the expense of a poorer match to the local luminosity function) would boost the number of high redshift galaxies.

The conclusion to be drawn from Table 2 is that it is possible to reproduce the observed number of Lyman-break galaxies, 1400 ± 300 per square degree, in a variety of cosmological models by reasonable adjustments to the input parameters. For example, within the observational errors, the standard CDM model produces the required abundance if the Miller-Scalo (Model A) or the Salpeter (Model C) IMF is assumed. Increasing the characteristic star formation timescale, $\tau_0^\star$, from 1.5 Gyr to 2 Gyr decreases the number of Lyman-break galaxies by about a factor two. Similarly, the open model F with a Miller-Scalo IMF is acceptable. The flat low-Ω models G and H produce about 2 to 3 times as many Lyman-break galaxies as observed. These abundances would be reduced, however, if the Miller-Scalo IMF were replaced by the Scalo IMF or if $\tau_0^\star$ were increased. Model D, the standard CDM cosmology with density fluctuations normalised to reproduce the observed abundance of rich clusters (Eke et al. 1996) produces far too few Lyman-break galaxies. However it would be premature to conclude that a standard CDM model with this normalization is incompatible with the high redshift data. For example a simple modification of the Cole et al. (1994) star formation rules, in which the timescale $\tau_0^\star$ is scaled with the dynamical time of the galaxy ($\tau_0^\star \propto (1+z)^{3/2}$) instead of remaining constant with redshift, results in an increase of $\mathcal{N}(\text{colour} + U_n)$ from 80 to 1900, without significant change in the properties of galaxies at the present time. We plan to explore the effects of such variations in the modelling of star formation and feedback in a future paper (Cole et al. in preparation). Note that not all the models listed in Table 2 reproduce the total counts of galaxies brighter than $\mathcal{R}_{AB} = 25$ quoted by Steidel et al. (1995). However, as mentioned above, these counts may be uncertain by a significant factor.

Our predicted redshift distribution for Lyman-break galaxies after the various selection criteria have been applied is shown in Fig. 2. Only galaxies brighter than $\mathcal{R}_{AB} = 25$ are included in this plot. As was evident from Fig. 1, the Steidel et al. (1995) colour criteria allow a significant population of galaxies with redshifts just below 3. Introducing a U_n-band detection limit biases the sample against the highest redshift galaxies whose light experiences the most absorption by intervening cold gas, skewing the distribution of robust candidates towards $z \sim 3$. The top panel of Fig. 2 shows results for our standard CDM model A and the bottom panel compares these with results from the flat low-Ω model G. The two distributions, heavily constrained by the selection criteria, are very similar.

Fig. 3 shows the number counts of galaxies predicted in two of our models. In Fig. 3a, the solid lines refer to model A and the dotted lines to model G. The higher amplitude

pair of curves gives the total number counts in these two models while the lower amplitude curves give the number of objects that satisfy the Steidel et al. $U_n - G$, $G - \mathcal{R}$ colour criteria. The fraction of the total counts represented by Lyman-break galaxies increases rapidly with increasing magnitude. The counts in model A are shown in more detail in Fig. 3b. Again, the high amplitude solid curve gives the total counts while the dotted line shows the number of galaxies that satisfy the colour selection criteria. The counts of galaxies with redshifts in the range $3.0 < z < 3.5$ are indicated by the short-dashed line and the counts at $4.0 < z < 4.5$ are shown by the long dashed line. The latter are lower by about one order of magnitude.

Steidel et al. (1996b) and Madau et al. (1996) have applied a similar technique to isolate high redshift galaxies in the Hubble Deep Field (Williams et al. 1996). The HDF was imaged in four passbands and so two-colour selection can be applied to select galaxies that 'drop out' in two passbands, U_{300} and B_{450}. The U_{300} dropouts are predicted to lie in the redshift range $2.0 < z < 3.5$ whilst the B_{450} dropouts should have redshifts between $3.5 < z < 4.5$ (Madau et al. 1996). We have made mock HDF catalogues from the output of our model, using the same filters and applying the detailed colour selection given by Madau et al. A comparison of the abundance of high redshift objects with the inferred abundances for the HDF is given in Tables 3 and 4. In Table 3 we consider galaxies brighter than $V_{606} = 28.0$ and $B_{450} = 26.8$, while, in Table 4, we consider galaxies brighter than $V_{606} = 27.7$. These data lead to a similar conclusion as the data in Table 2: several of our models (as did the some of the more successful models of White & Frenk 1991) predict approximately the observed abundance of high redshift galaxies thoughout the redshift range $2.0 < z < 4.5$. Our predicted abundances are sensitive to the IMF assumed – model B with a Scalo IMF gives seven times fewer B_{450} dropouts compared with model A which uses a Miller-Scalo IMF.

3.3. *Properties of high redshift galaxies*

In this Section we consider the properties of galaxies in models A and G that satisfy the Steidel et al. colour selection criteria and that are brighter than $\mathcal{R}_{AB} = 25.0$; we do not apply any conditions on their U_n magnitudes.

3.3.1. *Dark matter halos*

The masses of the dark matter halos that harbour Lyman-break galaxies brighter than $\mathcal{R}_{AB} = 25.0$ and the circular velocities of the halos in which these galaxies formed are plotted in Fig. 4. The solid lines correspond to the standard CDM model A, and the dashed lines to the flat, low-Ω model G. The halo masses plotted in the top panel are remarkably similar in the two cosmologies. This is largely a coincidence arising from the interplay between the selection criteria imposed on the galaxies and the overall halo mass distributions in the two cosmologies. The circular velocities plotted in the bottom panel are also similar, with a shift towards lower values in the low-Ω cosmology.

S96 estimated velocity dispersions for the Lyman-break galaxies from the widths of heavily saturated interstellar absorption lines. As they point out, these measurements may be contaminated by turbulent motions in the

TABLE 3

Comparison of the abundance of high redshift galaxies in models A and G with the abundances inferred from the Hubble Deep Field by Madau et al. (1996). Madau et al. estimate that the U_{300}-band dropouts lie in the redshift range $2.0 < z < 3.5$ and the B_{450}-band dropouts in the redshift range $3.5 < z < 4.5$. This Table refers to U_{300}-band dropouts, whilst Table 4 refers to B_{450}-band dropouts. The values in the table give the number of objects per square degree. The final column gives the number of colour selected objects as a percentage of the total number of objects in the sample.

model	$\mathcal{N}_{tot}(B_{450} < 26.8)$	$\mathcal{N}(2.0 < z < 3.5)$	$\mathcal{N}(\text{colour})$	% of $\mathcal{N}_{tot}$
A	360×10^3	54×10^3	66×10^3	18
G	290×10^3	65×10^3	79×10^3	27
observed	$(320 \pm 16) \times 10^3$	-	$(46 \pm 6) \times 10^3$	14

TABLE 4

Comparison of the abundance of high redshift galaxies in models A and G with the abundances inferred from the Hubble Deep Field by Madau et al. (1996) for B_{450}-band dropouts.

model	$\mathcal{N}_{tot}(V_{606} < 27.7)$	$\mathcal{N}(3.5 < z < 4.5)$	$\mathcal{N}(\text{colour})$	% of $\mathcal{N}_{tot}$
A	790×10^3	9.9×10^3	5.9×10^3	0.7
G	620×10^3	16×10^3	9.4×10^3	1.5
observed	$(620 \pm 20) \times 10^3$	-	$(9.3 \pm 2.5) \times 10^3$	1.5

gas. Alternatively, they may be due entirely to gravitationally supported random motions and, in this case, their measurements indicate velocity dispersions in the range $\sigma_{1D} = 180 - 320\,\mathrm{km\,s^{-1}}$, corresponding to circular velocities $V_c = \sqrt{2}\sigma_{1D} = 250 - 450\,\mathrm{km\,s^{-1}}$. If the line widths are due to rotational motion in a disk of constant circular velocity, V_c, then the observed range of full-width at half-maximum, $400 - 700\,\mathrm{km\,s^{-1}}$, corresponds to $V_c \approx 250 - 430\,\mathrm{km\,s^{-1}}$ for randomly oriented disks. Our model predictions in both cosmologies, illustrated in Fig. 4, are consistent with these numbers. Note, however, that the circular velocities plotted in the Figure are asymptotic halo values. The actual circular velocity is a function of radius. This, as well as the redistribution of mass associated with the formation of the galaxy, will affect what can be measured observationally. In principle, these can be substantially different from the asymptotic halo values. We intend to explore this issue in detail in a subsequent paper.
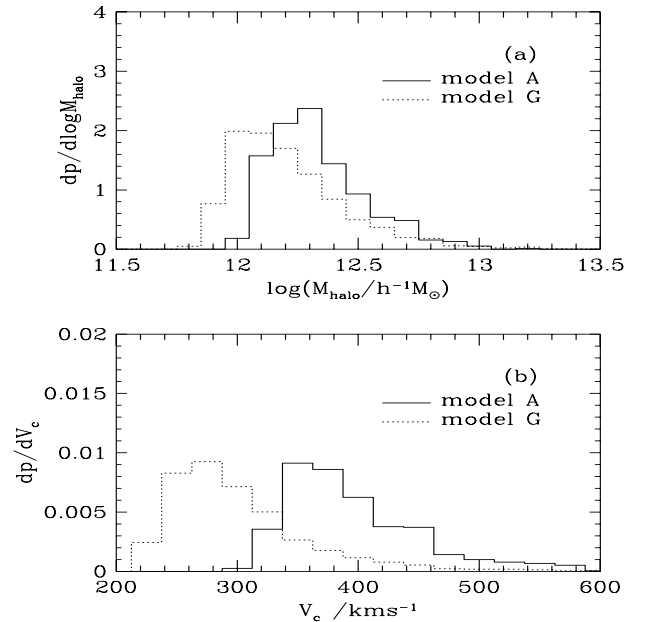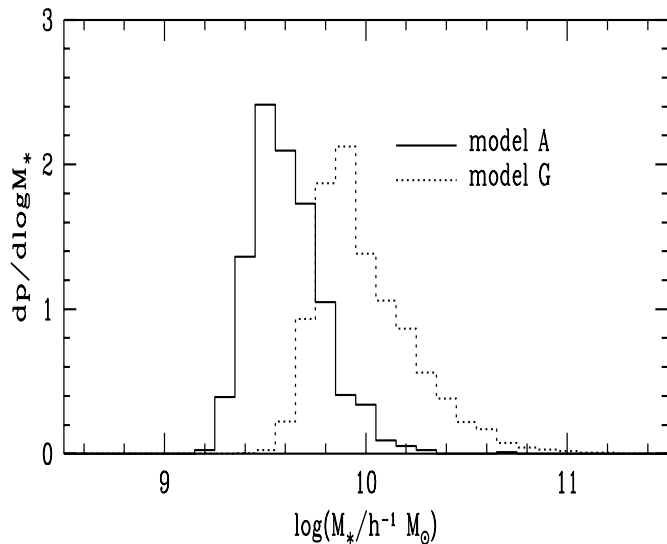

FIG. 4 Masses and circular velocities of the dark matter halos that harbour Lyman-break galaxies. Galaxies brighter than $\mathcal{R}_{AB} = 25.0$ satisfying the colour criteria of Steidel et al. (1995) are included. The solid lines show the distributions for the standard CDM model A, whilst the dotted lines show distributions for the flat low-Ω model G. The top panel gives the distribution of halo masses, and the bottom panel the distri-

bution of circular velocities for the halos in which each galaxy formed.

3.3.2. *Stellar masses and star formation rates*

The stellar masses of our model Lyman-break galaxies brighter than $\mathcal{R}_{AB} = 25.0$ are plotted in Fig. 5. As before, the solid line shows results for the $\Omega_0 = 1$ model A and the dotted line for the flat, low-Ω model G. The stellar masses are typically three times larger in the low-Ω cosmology. This difference is the result of the selection criteria imposed on these galaxies: luminosity distances are larger in the low density model, so galaxies selected at a given apparent magnitude limit must have larger luminosities, and thus larger stellar masses.

An indication of the stellar masses of real Lyman-break galaxies comes from K-band imaging of 5 candidate UV dropouts carried out by S96 at the Keck telescope. For these 5 candidates, they find $K_{AB} = 23.2 - 24.0$, and colours $0.4 \leq (\mathcal{R}_{AB} - K_{AB}) \leq 1.3$. Galaxies in our models have K magnitudes in the range $K_{AB} = 22 - 24$, with colours in the range $0.5 \leq \mathcal{R}_{AB} - K_{AB} \leq 1.4$, in excellent agreement with the data, as shown in Fig. 6.

FIG. 5 The stellar mass distribution of Lyman-break galaxies. Galaxies brighter than $\mathcal{R}_{AB} = 25.0$ satisfying the colour criteria of Steidel et al. (1995) are included. The $\Omega_0 = 1$ model A is shown by the solid line and the low-Ω model G by the dotted line.
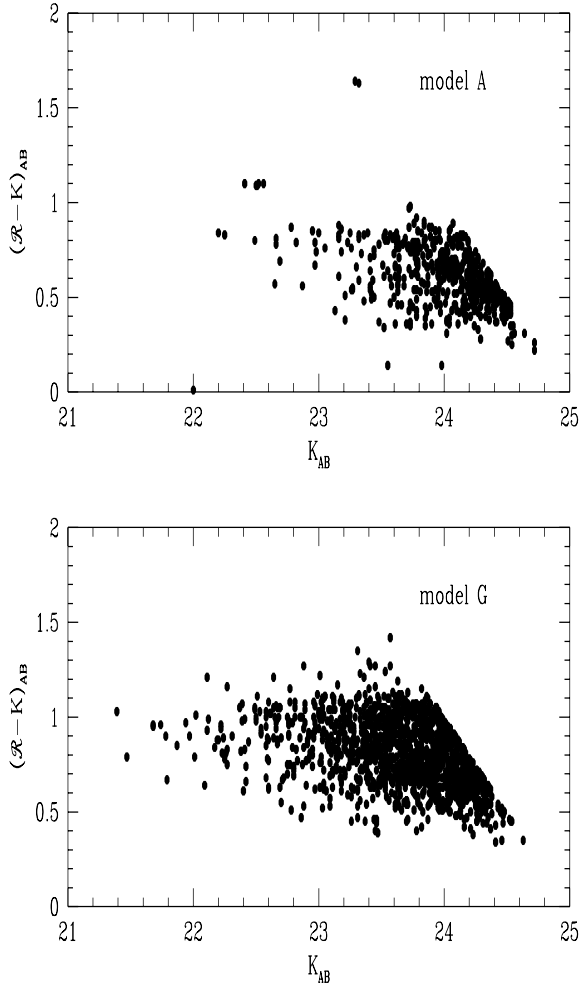
The distribution of star formation rates in our model Lyman-break galaxies is shown in Fig. 7a. These are instantaneous rates, measured directly from the mass of cold gas turned into stars per unit time. The star formation rates at $z \simeq 3$ are typically a few solar masses per year, and are somewhat larger in the flat low-Ω model than in the standard model. Only a very small fraction of the galaxies at these redshifts have star formation rates in excess of $10h^{-2}\mathrm{M}_\odot\mathrm{yr}^{-1}$. The instantaneous star forma-

tion rates in typical galaxies at $z \simeq 3$ are comparable to their mean rates averaged over the age of the universe at that redshift (1.6 Gyr in model A, 2.5 Gyr in model G). We consider the history of star formation in more detail in Section 5.

Whereas the star formation rate of a galaxy is not directly observable, the distribution of $\mathcal{R}$ magnitudes is. Since the $\mathcal{R}$ band samples the rest frame ultraviolet at $z \simeq 3$, the distribution of $\mathcal{R}$ magnitudes is closely related to the distribution of star formation rates. In Fig. 7b we plot the distribution of absolute magnitude $M_R(AB)$ in our models. This distribution, however, is not a particularly strong constraint on the models because, by design, the S96 survey covers only a narrow range in $\mathcal{R}_{AB}$. We defer a detailed comparison between our predicted star formation rates and observations to Section 5.

3.3.3. *Galaxy sizes*

An essential feature of hierarchical models of galaxy formation is that the typical sizes of galaxies increase with time. Thus, we expect the characteristic radii of galaxies to be considerably smaller at high redshift than they are at present. A detailed investigation of the evolution of galactic sizes will be presented elsewhere (Lacey et al. in preparation). A rough indication of the sizes of high redshift galaxies, however, may be obtained from a simple model assuming that galaxies acquire their angular momentum from tidal torques and that the angular momentum of the gas is conserved as it condenses within its halo.

FIG. 6 The predicted $(\mathcal{R} - K)_{AB}$ colour distribution of galaxies brighter than $\mathcal{R}_{AB} = 25.0$ satisfying the Steidel et al. colour selection. The top panel shows model A and the lower panel shows model G.
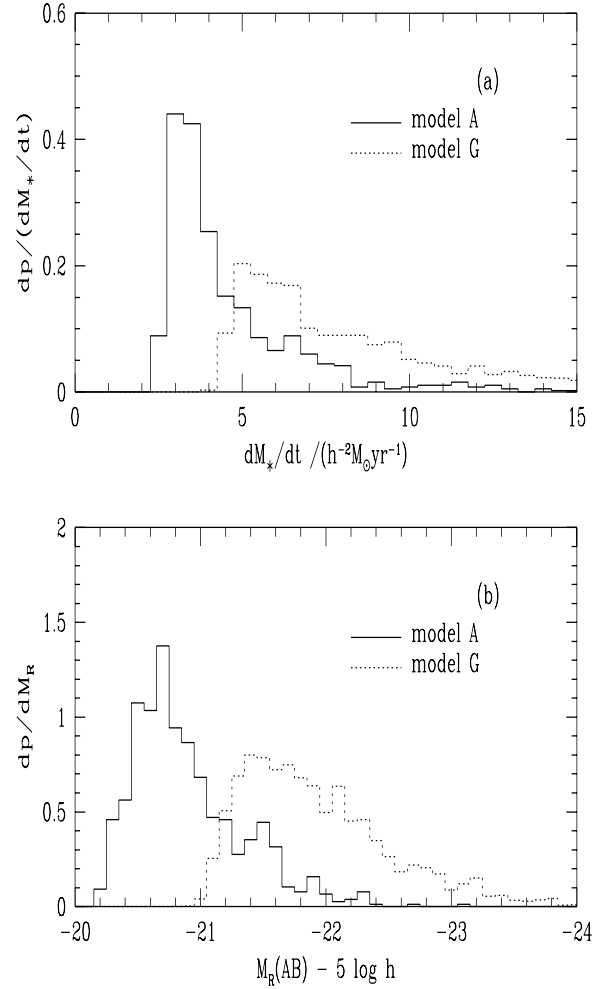
FIG. 7 Star formation rates and absolute $\mathcal{R}_{AB}$ magnitudes for high redshift galaxies. Galaxies with apparent magnitudes $\mathcal{R}_{AB} < 25.0$ satisfying the colour criteria of Steidel et al. (1995) are included. Model A is shown by the solid line and model G by the dotted line. The top panel gives the distribution of instantaneous star formation rates in the models and the bottom panel the distribution of absolute magnitudes, $M_{\mathcal{R}}$.

This simple model is quite adequate because, as we discuss in Section 4, high redshift galaxies in our model tend to have very small bulges or no bulge at all. From this simple model, we obtain half light radii $r_{\rm h} \sim 0.4h^{-1}$kpc at $z \simeq 3$ in model A and $r_{\rm h} \sim 0.6h^{-1}$kpc in model G. This rough calculation agrees reasonably well with the values of $r_{\rm h} \simeq 0.7 - 1.0h^{-1}$kpc ($\Omega_0 = 1$) or $r_{\rm h} \simeq 1.0 - 1.5h^{-1}$kpc ($\Omega_0 = 0.3$, $\Lambda_0 = 0.7$) measured by Giavalisco, Steidel & Macchetto (1996) from HST follow-up observations of S96 Lyman-break galaxies.
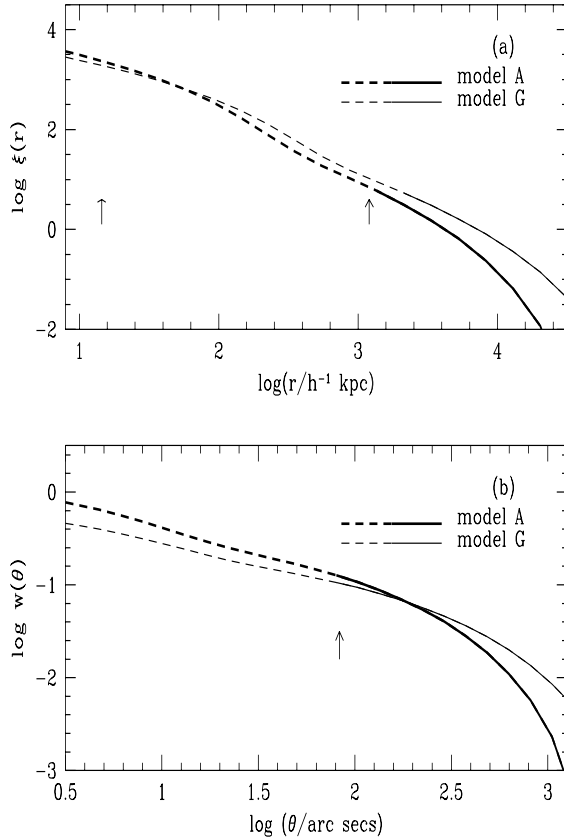
3.3.4. Clustering properties

We calculate the expected clustering of high redshift galaxies in two basic steps. First, we calculate the non-linear power spectrum $P(k, z)$ of fluctuations in the *mass distribution* in comoving coordinates, using the approx-

imate linear to non-linear transformation of Peacock & Dodds (1996). Next, we obtain a bias parameter for the galaxies using the prescription of Mo & White (1996). This gives the bias of dark matter halos of mass M at redshift z as

$$b(M, z) = 1 + \frac{1}{D(z)\delta_c(z)} \left[\frac{\delta_c^2(z)}{\sigma^2(M)} - 1 \right], \qquad (1)$$

where $\sigma(M)$ is the rms linear density fluctuation at $z = 0$ in a sphere of mass M, $D(z)$ is the linear growth factor, and $\delta_c(z)$ is the extrapolated critical linear overdensity for collapse at redshift z.

In the model, the majority of the Lyman-break galaxies are the central galaxy in their dark matter halo. A good approximation to the galaxy bias function is the mean halo bias, $\bar{b}$, weighted according to the mass distribution of halos that harbour galaxies satisfying the Steidel et al. (1995) colour selection criteria (c.f. Fig. 4). The power spectrum of the Lyman-break galaxies is then given by $P_{\rm gal}(k, z) = \bar{b}^2 P(k, z)$. From equation (1), we find $\bar{b} = 4.2$ in model A and $\bar{b} = 3.5$ in model G, making the approximation that the halos all lie at the median redshift $z_{\rm m}$ of the colour selected sample.

The spatial correlation function $\xi(r)$ of the high redshift galaxies is obtained by taking the Fourier transform of the power spectrum $P_{\rm gal}(k, z)$. The angular correlation function $w(\theta)$ can be calculated using the relativistic version of Limber's (1954) equation in the form derived by Baugh & Efstathiou (1993). We make the approximation that the evolution of clustering and the bias parameter are negligible over the narrow range of redshifts in which Lyman-break galaxies satisfying the S96 criteria are found, so that $P_{\rm gal}(k, z) \simeq P_{\rm gal}(k, z_{\rm m})$ in the integral. The relativistic Limber equation can then be written as:

$$w(\theta) = \int k \, P_{\rm gal}(k, z_{\rm m}) \, g(k\theta) \, {\rm d}k, \qquad (2)$$

The kernel function is given by:

$$g(k\theta) = \frac{1}{2\pi} \frac{1}{N^2} \int_0^\infty F(x) \left(\frac{{\rm d}N}{{\rm d}z} \right)^2 \frac{{\rm d}z}{{\rm d}x} J_0(k\theta x) \, {\rm d}z, \qquad (3)$$

where x is the comoving distance to redshift z. The term $F(x)$ comes from the metric and depends on the cosmology (e.g. Peebles 1980 §56); in a flat universe $F(x) = 1$. The redshift distribution dN/dz is that of the colour-selected galaxies, and N is the total number of galaxies selected. The spatial and angular correlation functions for galaxies satisfying the Steidel et al. selection are shown in Fig. 8a and Fig. 8b.

The derivation of the formula for the halo bias, equation (1), by Mo & White (1996) formally assumes that the correlation function of the matter satisfies $\xi_{\rm m}(r) \lesssim 1$ and that $r \gtrsim r_{\rm L}/2$, where $r_{\rm L} = (3M/4\pi\rho_0)^{1/3}$ is the comoving Lagrangian radius of the halos (ρ_0 being the present mean density). The model has been tested against N-body simulations by Mo & White and by Mo, Jing & White (1996), who find that the formula works quite well in practice down to where $r \approx r_{\rm L}$, even when $\xi_{\rm m}(r) > 1$. For the Lyman-break galaxies in model A, $r_{\rm L} \sim 1h^{-1}{\rm Mpc}$ (comoving), corresponding to $\theta \sim 70''$ for $z = 3$. Coincidentally, this is close to the scale where $\xi_m(r) = 1$. On smaller scales, the halo correlation function should flatten relative to the matter correlation function. In Fig. 8 we have therefore plotted the galaxy correlation function as a dashed curve on scales $r < r_{\rm L}$, where the assumption of constant bias probably breaks down. The spatial correlations in the range $0.3 \leq r \leq 3h^{-1}{\rm Mpc}$ (comoving) are a good match to a power-law, $\xi(r) = (r_0/r)^\gamma$, with $\gamma = 1.8$ and $r_0 = 3.9h^{-1}{\rm Mpc}$. Thus, our models predict that Lyman-break galaxies at $z = 3$ should have a comoving clustering length comparable to that of bright galaxies today.

FIG. 8 The clustering of the colour selected high redshift galaxies in our models. Panel (a) shows the predicted spatial correlation functions in comoving co-ordinates and panel (b) the predicted angular correlation functions. The heavy and light lines correspond to correlations computed from the non-linear power spectrum in models A and G respectively, after multiplication by the bias parameter of the halos: for model A, $\bar{b} = 4.2$ and for model G, $\bar{b} = 3.5$. The solid lines show the scales at which the assumption of a constant bias parameter is expected to be valid. The extrapolation of a constant bias to scales smaller than this is shown by broken lines. The arrow in (a) at $r = 14h^{-1}{\rm kpc}$ marks the comoving scale represented by 1 arcsecond at $z = 3$. The second arrow, at $r = 1.1h^{-1}{\rm Mpc}$ indicates the comoving size of a region that collapses to form an object with the median halo mass found for the colour selected galaxies in model A. The angular scale corresponding to this comoving length, 70 arcseconds in model A, is shown by the arrow in (b).

We see that the models predict appreciable angular correlations for the Lyman-break galaxies, $w(\theta) \approx 0.1$ at $\theta = 100''$ for model A, and a slightly lower value for model G. In contrast, Brainerd et al. (1995) estimated $w(\theta) \approx 0.005$ at the same angular scale for field galaxies with $\mathcal{R}_{AB} \lesssim 25$. The larger $w(\theta)$ that we predict is the result of several effects: (i) the relatively narrow redshift range for the Lyman-break objects, which reduces projection effects in $w(\theta)$; (ii) the large degree of bias, $\bar{b} \sim 4$, which results from the galaxies occuring in rare dark halos; and (iii) possible differences in the R magnitude scale between the S96 and Brainerd et al. datasets.

4. THE FATE OF HIGH-Z GALAXIES

In Section 3 we showed that a population of star forming galaxies with the abundance and global properties of the Lyman-break galaxies discovered by S96 arise naturally in hierarchical clustering theories. Models with a range of values of the cosmological parameters are equally successful in accounting for this population of high redshift galaxies. In this and the following section we consider the role that this population plays in the general scheme of galaxy formation. First we ask the question: what do the Lyman-break galaxies evolve into? Are they, as S96 conjectured, the progenitors of the spheroidal components of present day galaxies? Our semi-analytic modelling technique provides an ideal tool to answer this sort of question since the entire evolutionary history of a model galaxy is readily available.

We begin by displaying graphically the evolutionary paths of a few examples. From the present day population in the model, we have chosen four examples of different morphological types with at least one progenitor at $z \approx 3$ that satisfied the S96 colour and magnitude selection criteria. The tree plots in Fig. 9 illustrate the star formation histories of these examples. The stellar mass of the final, present day, galaxy is given at the top of each panel, along with the B-band luminosity, bulge-to-total luminosity ratio in the B band and the B-V colour. Redshift decreases down the trees, and the bottom of each plot represents the present day. Each branch in the tree represents a progenitor fragment and its width at any epoch is proportional to the mass of stars in the progenitor at that epoch. Branches merge together when the fragments they represent merge. The plots have been normalised to have unit width at $z = 0$. These tree plots are similar to those used by Baugh, Cole & Frenk (1996b) to illustrate the formation paths of galaxies of different morphological types (see their figures 2 and 3.) Galaxies that undergo major mergers at recent epochs are identified with ellipticals and S0s whereas galaxies that have grown quiescently by protracted accretion of cooling gas (perhaps around a bulge formed by a prior merger) are identified with spirals. Minor mergers that do not disrupt a stellar disk add stars to the bulge component (see Baugh et al. 1996b for precise definitions.)

At the present day, the galaxy in the top left hand corner of Fig. 9 is a spiral, the galaxy at the bottom left is on the border between being an elliptical or S0 galaxy, the galaxy at the top right is a field elliptical and the galaxy at the bottom right is a cluster elliptical. Lyman-break galaxies (marked by the star in each panel) can therefore end up

in galaxies of any morphological type and, as we shall see in Fig. 11, they can span a wide range of luminosity.

The distribution of bulge-to-total stellar mass amongst the descendants of Lyman-break galaxies is similar to that of bright galaxies ($M_B - 5 \log h = -19$) without such a progenitor. The distribution of halo circular velocity for the Lyman-break descendants, on the other hand, is biased towards large values typical of groups and clusters (Fig. 10). This is just what was expected in view of the strong clustering bias exhibited by the Lyman-break galaxies themselves (see §3.3.4).

The luminosity function of the present day descendants of Lyman-break galaxies is plotted in Fig. 11 where it is compared with the luminosity function of the galaxy population as a whole. In this figure we show results for both the standard CDM model A and the low-Ω model G. In both cases, the bright end of the current luminosity function is made up of galaxies which, at $z \simeq 3$ had at least one progenitor that satisfied the luminosity and colour criteria required to qualify as a Lyman-break galaxy in the study of Steidel et al. (1995). Virtually all present day galaxies with $L \gtrsim 2.5 L_*$ have such a progenitor. The fraction of Lyman-break descendants decreases with decreasing luminosity so that virtually no present day galaxy with $L \lesssim L_*/5$ was ever a Lyman-break galaxy of the type observed by Steidel et al.

The assembly of the Lyman-break galaxies themselves is illustrated in Fig. 12 where we plot the growth of the stellar mass of selected Lyman-break galaxies with time. The stellar mass at each redshift (which may be spread amongst several fragments) is plotted as a fraction of the "final" stellar mass of the Lyman-break galaxy at $z = 3$ in Fig. 12(a). Star formation in the Lyman-break galaxies begins very early, at $z > 6$, but only $\sim 20 - 40\%$ of the stars have formed by $z = 4$. The bulk of the stars present in these Lyman-break galaxies at $z \simeq 3$ was formed in the preceeding few hundred million years. The total star formation rates summed over the fragments, in units of the star formation rate at $z = 3$, are plotted in Fig. 12(b).
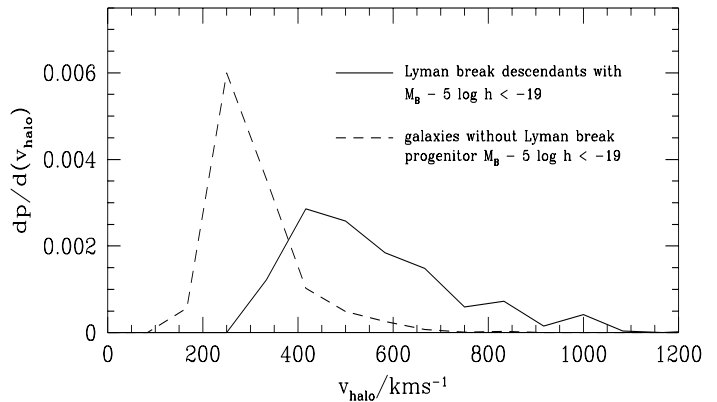

FIG. 10 The distribution of present-day halo circular velocity of galaxies in model A that contained at least one Lyman-break galaxy at high redshift (solid line), compared with the
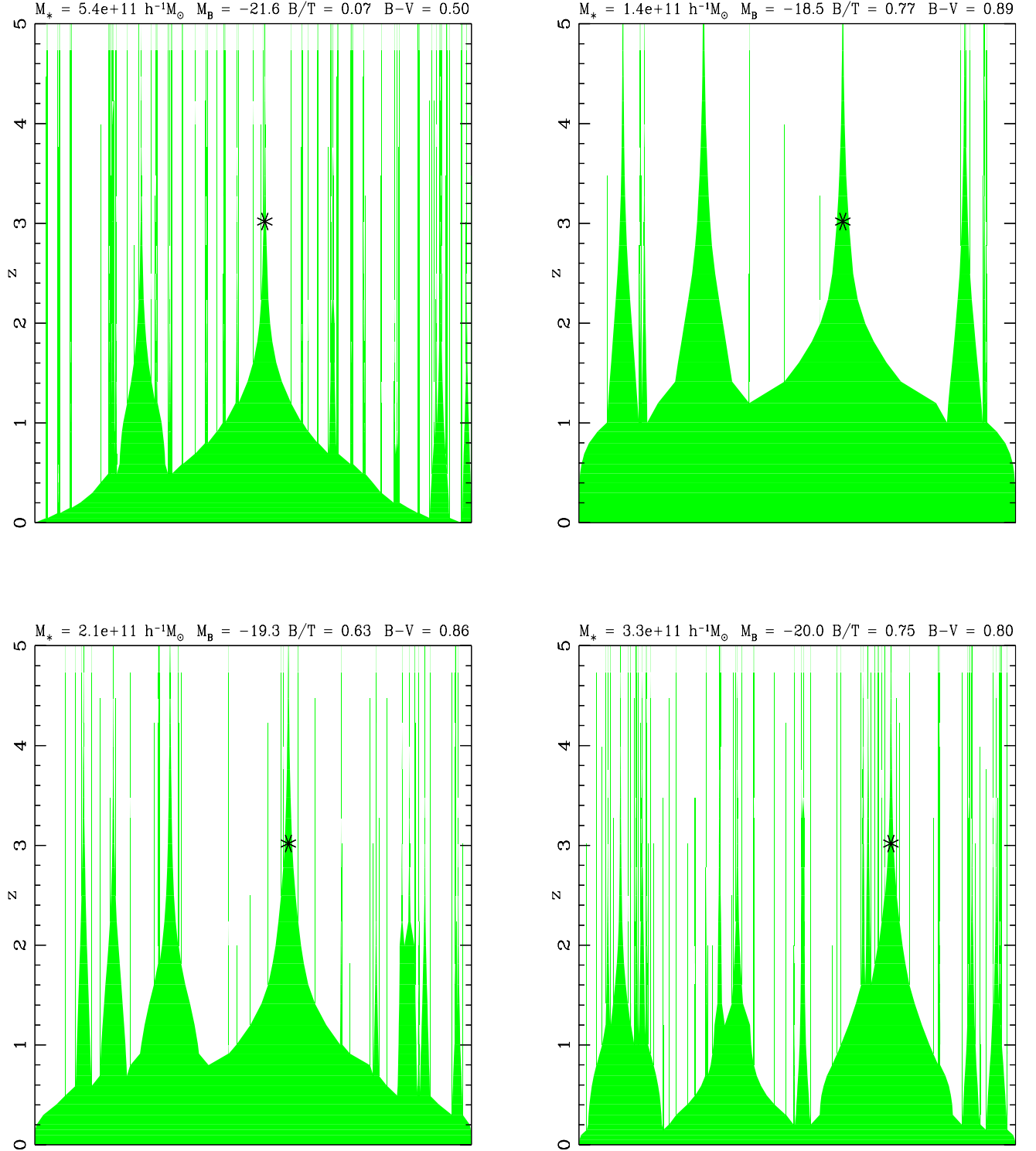
FIG. 9 Tree diagrams illustrating the star formation histories of four present day galaxies which had a high redshift progenitor satisfying the luminosity and colour selection criteria of Steidel et al. (1995). The actual progenitor is marked by a star. These examples are taken from the standard CDM model A. The present day is at the base of each tree - the trees extend back to a redshift of 5. The width of each branch at any epoch is proportional to the mass in stars in the branch at that epoch. The trees have been normalised to have unit width at $z = 0$. The labels give the stellar mass of the final galaxy at the present day, along with its B band luminosity, the bulge to total light ratio in the B band and the B-V colour.

distribution of halo velocities for present day galaxies without such a progenitor (dashed line). All the present day galaxies considered are brighter than $M_B - 5 \log h = -19$.
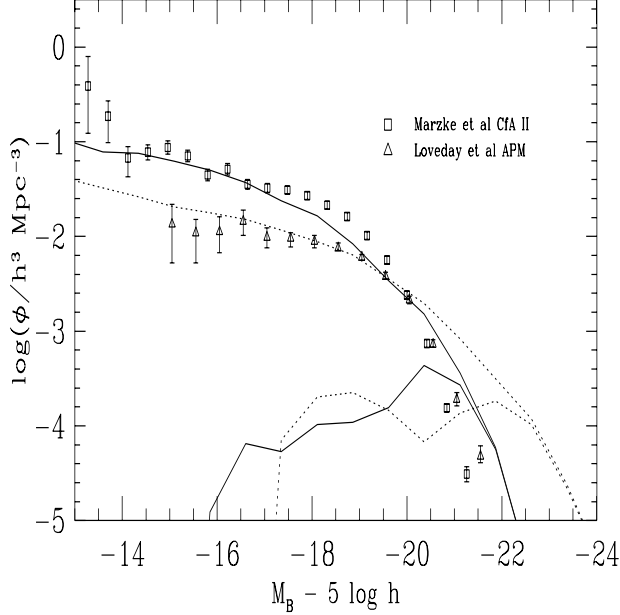
FIG. 11 Present-day B-band luminosity functions in model A (solid lines) and model G (dotted lines). In each case, the extended curve shows the luminosity function of the galaxy population as a whole. The shorter curve shows the luminosity function of galaxies that contained at least one progenitor satisfying the selection criteria for Lyman-break galaxies at high redshift in the study of Steidel et al. (1995). The data points show observational determinations of the luminosity function from Loveday et al. (1992) and Marzke et al. (1994).
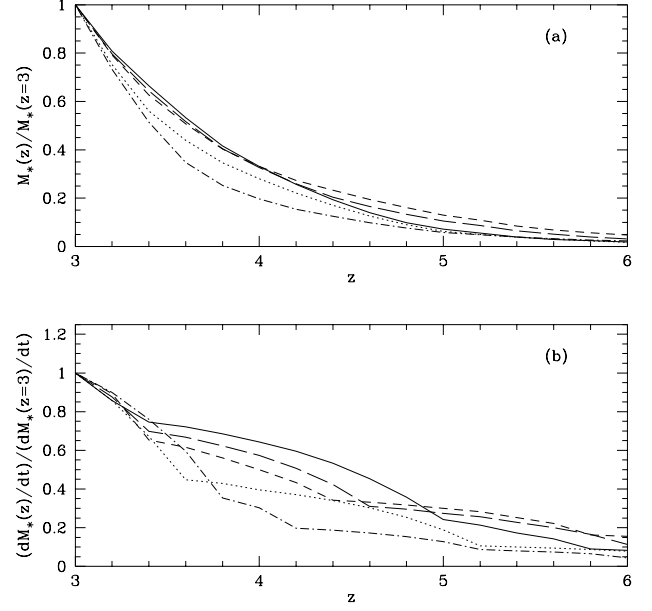
FIG. 12 The star formation histories of five example galaxies that satisfy the Steidel et al. colour selection in model A. The galaxies all have dark halos of mass $2 \times 10^{12} h^{-1} M_\odot$ at $z = 3$. Panel (a) shows the build up in stellar mass expressed as a fraction of the mass in stars at $z = 3$. Panel (b) shows the instantaneous star formation rate in units of the star formation rate at $z = 3$. Curves of the same line style refer to the same galaxies in (a) and (b).
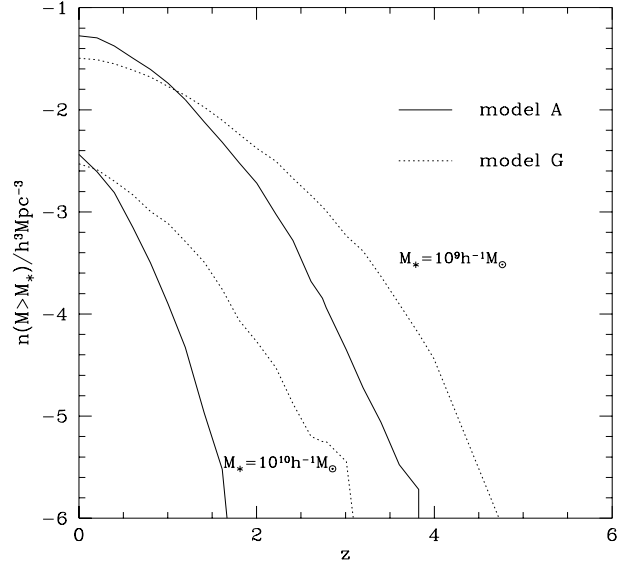

FIG. 13 Evolution of the comoving number density of galaxies that have stellar masses in excess of 10^9 and $10^{10} h^{-1} M_\odot$. The solid line shows results for model A and the dotted line for model G.

The build-up of the population of galaxies with masses typical of Lyman-break galaxies is illustrated in Fig. 13. Here we plot the evolution of the comoving number density of galaxies that have stellar masses in excess of 10^9
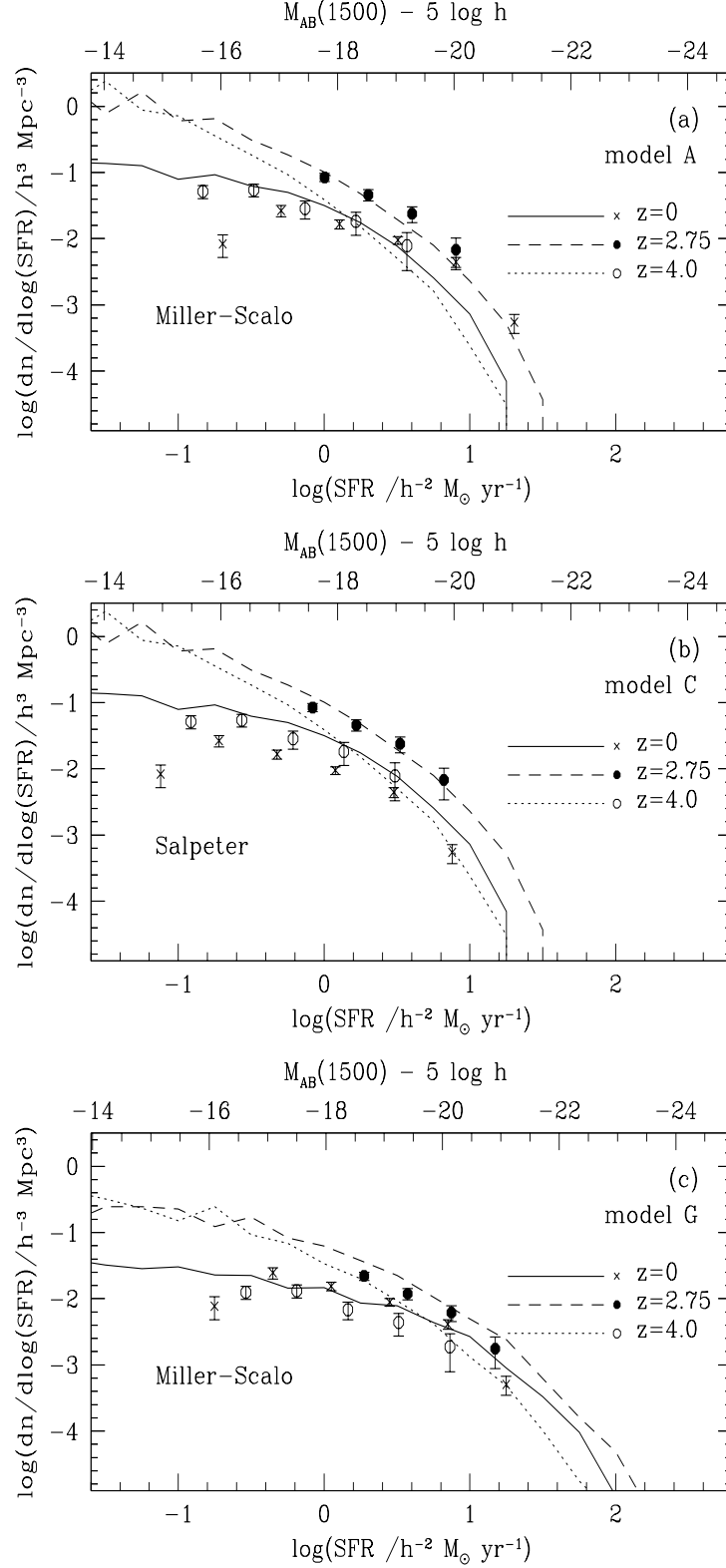
FIG. 15 The distribution of star formation rates (number of star forming systems per $\log_{10}(SFR)$ per comoving volume) at different redshifts, computed from our models and compared to observational data. Panel (a) shows model A, panel (b) model C and panel (c) model G. The solid, dashed and dotted lines show the model predictions for $z = 0, 2.75$ and 4 respectively. The symbols with error bars are observational data points. The crosses are for $z = 0$ (Gallego et al. 1995), the filled circles for $\langle z \rangle = 2.75$ (Madau 1996) and the open circles for $\langle z \rangle = 4$ (Madau 1996). The observational data have been converted into total SFRs assuming either a Miller-Scalo or Salpeter IMF, as indicated on each panel and described in the text. The top scale shows the luminosity $L(1500)$ expressed as an AB magnitude: $M_{\rm AB}(1500) = -2.5 \log(L(1500)/{\rm erg\, s^{-1} Hz^{-1}}) + 51.6$.
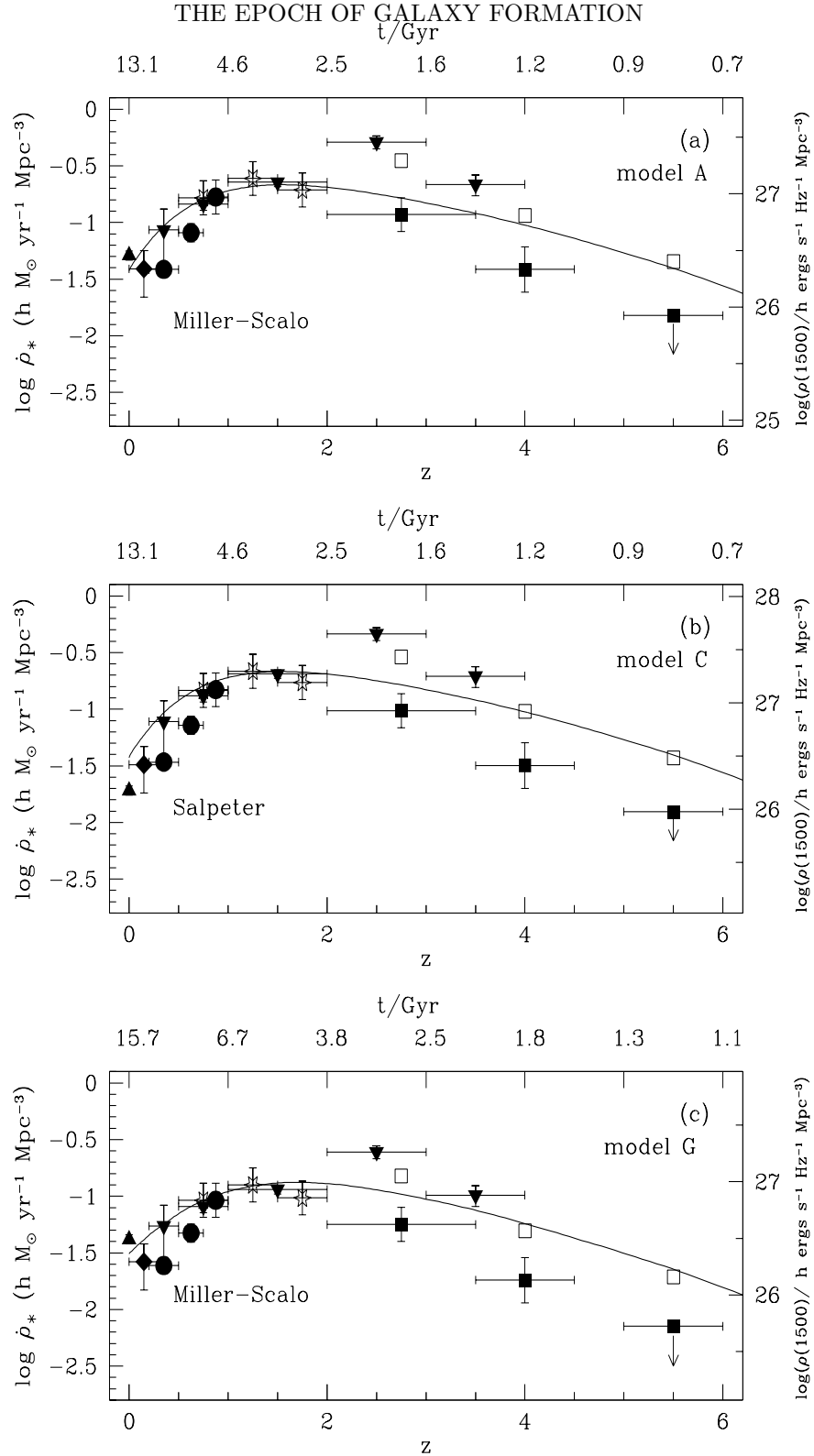
FIG. 16 The total star formation rate per comoving volume as a function of redshift, computed from our models (solid curves) and compared to observational estimates (symbols). Panel (a) is for model A, panel (b) for model C and panel (c) for model G. The filled triangle is based on the Hα luminosity function of Gallego et al. (1995); the filled diamond is from the 2000Å luminosity function of Treyer et al. (1997); the filled circles are from the rest frame 2800Å luminosity densities of Lilly et al. (1996); the open stars come from the 2800Å fluxes of Connolly et al. (1997); the inverted triangles are from the 3000Å fluxes of Sawicki et al. (1997); and the filled squares come from the 1500Å luminosity function of Madau (1996). The right hand scale shows the luminosity density at 1500Å. The data points have been converted to total star formation rates assuming either a Miller-Scalo or Salpeter IMF as indicated on each panel. The open squares show the effects of a factor of 3 correction in Madau's (1996), $z > 2$, star formation rates per unit comoving volume due to dust obscuration, as suggested by Pettini et al. (1997).

and $10^{10}h^{-1}M_{\odot}$. The number of galaxies above a given mass limit increases as star formation procedes, but it decreases when mergers involving galaxies of this size occur. At $z \simeq 3$, the abundance of galaxies with mass of a few times $10^{9}h^{-1}M_{\odot}$ is rapidly rising. This is also close to the time when galaxies of $M_{\star} = 10^{10}h^{-1}M_{\odot}$ first appear in significant numbers. Thus, in the cosmological models discussed in this paper, $z \simeq 3$ is the first epoch at which galaxies form with stellar masses comparable to present-day $L_{\star}$ galaxies.

FIG. 14 Predicted star formation histories in model A (solid line) and model G (dotted line). The curves give the fraction of the final mass in stars that has formed by a given redshift.

5. THE COSMIC STAR FORMATION HISTORY

White & Frenk (1991), Lacey et al. (1993), Cole et al. (1994) and Heyl et al. (1995) demonstrated that hierarchical models of galaxy formation that are consistent with local data tend to form the bulk of their stars at relatively low redshifts (see also Baron & White 1987). This is a feature not only of the $\Omega_0 = 1$ CDM cosmology, but also of successful low-density CDM models. Fig. 14 shows the star formation histories predicted in our $\Omega_0 = 1$ and low-Ω models (models A and G, indicated by solid and dotted lines respectively). In both cosmologies, 50% of the stars form after $z \simeq 1$. The stars that have formed by $z \simeq 3$ account for less than 10% of the present day total; very little star formation occurs before $z = 4$. Note that in spite of the improvements to our galaxy formation model, the curve for model A in Fig. 14 is virtually identical to the curve for the fiducial model in Figure 21 of Cole et al. (1994) while the curve for model G agrees well with the results tabulated in Table 3 of Heyl et al. (1995).

Observational data that can be compared with theoretical predictions for the cosmic star formation history are now becoming available (e.g. Lilly et al. 1996, Madau et al. 1996). In Fig. 15 we present a compilation of current data expressed as the comoving number density of galaxies as a function of star formation rate (SFR) at different redshifts. Star formation rates are not, of course, directly observed but inferred from the flux in a restframe UV passband, a cosmological model to convert flux to luminosity, a model for the spectral energy distribution, and an assumption about the initial stellar mass function (IMF). To intercompare different datasets amongst themselves and with our model predictions, we have derived SFRs from published data in a homogeneous manner. We present results for both the Miller-Scalo and Salpeter IMFs. The SFRs in our models are total and include the contribution from brown dwarfs (ie stars with mass below the hydrogen-burning limit) which is parametrized by the factor $\Upsilon > 1$ (see Table 1).
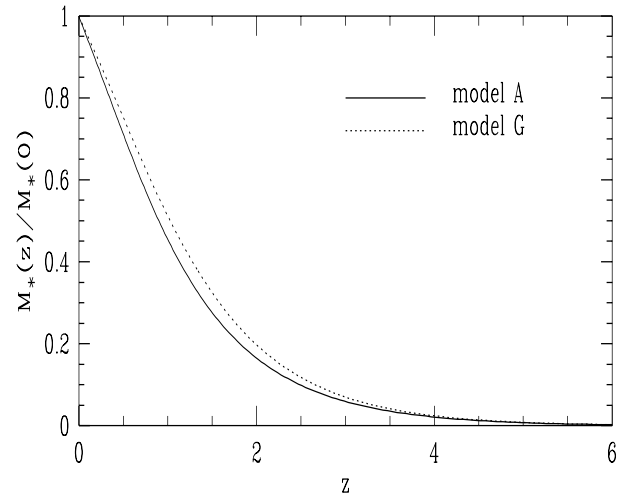
The $z = 0$ data plotted in Fig. 15 were derived from the Hα luminosity function of Gallego et al. (1995). The high-redshift data in the figure were derived from the data presented by Madau (1996) for galaxies in the Hubble Deep Field identified photometrically as Lyman-break galaxies. The U_{300}-band dropouts are estimated to have $2 < z < 3.5$ and $\langle z \rangle = 2.75$, while the B_{450}-band dropouts are estimated to have $3.5 < z < 4.5$ and $\langle z \rangle = 4$. Madau gives SFRs derived from broad-band magnitudes at wavelengths close to 1500Å in the rest frame. We first convert these back to the corresponding values of $L(1500) \equiv L_{\nu}(1500Å)$ using Madau's own conversion factor, as given in Madau et al. (1996). We then convert the 1500Å and Hα luminosities into total SFRs using the values tabulated in Table 5 and the appropriate value of Υ for each model. In addition, for models with $\Omega_0 \neq 1$ an approximate scaling has been applied to Madau's data points to account for the differences in the comoving volume element and luminosity distance in the different cosmologies.

The curves plotted on Fig. 15 display our model predictions. The upper panel shows results for our standard $\Omega_0 = 1$ model A and the lower panel for our flat low-Ω model G, both of which have the Miller-Scalo IMF. The middle panel shows model C which has $\Omega_0 = 1$ and the Salpeter rather than the Miller-Scalo IMF. The theoretical curves are exactly the same for this case as for model A, the only difference being the scalings applied to the observational data points. In all cases the behaviour of the models is qualitatively the same as the observed data. The SFRs are larger at the intermediate redshift $z = 2.75$ and at $z = 4$ they drop back to values similar to those at $z = 0$. The model that best reproduces the observed data is model A. There are, however, considerable uncertainties in this comparison. For example, the mean redshift of

TABLE 5

The $L(1500)$, $L(2800)$ and Hα luminosities produced by a constant total SFR $= \Upsilon M_\odot \text{yr}^{-1}$ after 1 Gyr. $L(H\alpha)$ in units of ergs s^{-1}, $L(1500)$ and $L(2800)$ in erg s^{-1}Hz^{-1}.

band	Miller-Scalo	Scalo	Salpeter
$L(H\alpha)$	1.38×10^{41}	6.21×10^{40}	1.98×10^{41}
$L(1500)$	1.34×10^{28}	3.88×10^{27}	8.68×10^{27}
$L(2800)$	1.12×10^{28}	3.59×10^{27}	6.76×10^{27}

the U_{300} dropouts in our mock HST catalogue is $z \simeq 2.3$, smaller than the central value, $\langle z \rangle = 2.75$, assumed for the real data. This approximation alone would lead to an overestimate of the inferred star formation rate by up to 15%. For the B_{450} dropouts this effect is smaller, around 5%. More importantly, these comparisons are sensitive to the details of the adopted IMF, as may be seen by the way in which the data points shift in panels a and b.

The cosmic star formation history may be conveniently summarised by considering the variation with redshift of the total SFR per comoving volume, as in the theoretical predictions of Fig. 14. This quantity is obtained by integrating the differential distributions in Fig. 15 over galaxies of all SFRs. For the theoretical models, this is straightforward, but for the observations, it involves extrapolating the distribution of SFRs to ranges not directly observed. Comparing theoretical and "observed" total SFRs is thus considerably more uncertain than comparing differential distributions. With this caveat, we compare in Fig. 16 our theoretical predictions with several observational estimates including those based on the data of Gallego et al. (1995) and Madau (1996) already described, and also the B-band data of Lilly et al. (1996) for $0.2 < z < 1$. In all cases, we have used the observers' estimates of the total luminosity density, which are based on fitting a Schechter function to the luminosity function and extrapolating it to all luminosities. The Lilly et al. data refer to the luminosity density at 2800Å. This is less directly related to the instantaneous star formation rate than the Hα or 1500Å luminosities, because it is dominated by somewhat older stars. The 2800Å rest-frame luminosity is sampled by the observed B-band flux only at $z \sim 0.5 - 1.0$, so the estimate at $z \sim 0.35$ requires a modest extrapolation from longer wavelengths. This introduces an additional uncertainty. The constants used to convert $L(2800)$ to total SFR are also listed in Table 5. The upper limit plotted at $z = 5.5$ is based on the number of V_{606} dropouts in the HDF, which are candidates to be Lyman-break galaxies at $5 < z < 6$ (Madau, private communication).

After the original version of this paper was submitted, many more data points have been added to the star formation history diagram and we reproduce here a selection of them. At low redshift, Treyer et al. (1997) have estimated the star formation density from 2000Å (rest-frame) fluxes; Sawicki et al. (1997) have used photometric redshifts of galaxies in the HDF to infer the star formation density from 3000Å fluxes; Connolly et al. (1997) have used both optical and ground based near-infrared imaging of the HDF to infer star formation rates from 2800Å fluxes. (The use of infrared data is particularly important for the accuracy of photometric redshifts at $z \sim 1-2$.) Apart from the Sawicki et al. points at $z > 2$, the level of agreement amongst these different determinations is remarkable, although it is suggestive that both the Sawicki et al. and Connolly et al. points at $z \leq 1$ lie above those from the CFRS survey, in better agreement with our model predictions. (The CFRS survey, however, has more galaxies and therefore smaller error bars at these redshifts.)

Overall, the agreement between theoretical predictions and data in Fig. 16 is impressive. It must be borne in mind that these are genuine theoretical predictions that predate the observational data. The theoretical curve in the upper panel of Fig. 16 is simply the time derivative of the integrated curve for the fiducial CDM model plotted in figure 21 of Cole et al. (1994). Note, however, that the location of the observational data points depends on the assumed IMF; Cole et al. used a Scalo IMF whereas in §3.2, we found a Miller-Scalo or Salpeter IMF to be preferable. For a given luminous star formation rate, SFR/Υ, a Miller-Scalo IMF gives 2.2 times the Hα flux, 3.5 times the 1500Å flux and 3.1 times the 2800Å flux compared to a Scalo IMF. Comparing panels (a) and (b) of Fig. 16, we see that the main effect of changing the IMF from Miller-Scalo to Salpeter is to move the $z = 0$ data point based on the Hα luminosity. Both models A and G show the same qualitative trend as the data, with a broad peak in the total SFR at $1 \lesssim z \lesssim 2$. For $z \gtrsim 2$, the model SFRs fall off somewhat more slowly than the data. The completeness of the observational data at these high redshifts, however, is difficult to establish.

A further source of uncertainty is the possible presence of dust in the star-forming galaxies. Even a modest amount of dust would cause attenuation of the ultraviolet flux, leading to a potentially severe underestimate of the star formation rate. Tentative detections of the cosmic infrared background by Puget et al. (1996) and Guiderdoni et al. (1997a) and upper limits on it (Kashlinsky, Mather & Odenwald 1996) provide only weak constraints on the amount of dust present in high redshift galaxies (Madau, Pozzetti & Dickinson, 1997; Guiderdoni et al. 1997b). Monolithic collapse models (e.g. Eggen, Lynden-Bell & Sandage 1962) in which a significant fraction of the total star formation in the universe takes place at high redshifts enshrouded in dust (e.g. Meurer et al. 1997),

appear to overpredict the total mass of heavy elements in place at early times (Madau et al. 1997), as inferred from observations of damped Lyman-α systems (Pettini, Smith, King & Hunstead 1997). Estimates of the factor by which star formation rates deduced from UV flux should be revised to account for the presence of dust span a range of values. The results are sensitive both to the form of the extinction law adopted and to the assumed age of the primeval galaxy which determines how intrinsically blue it is. Primeval galaxies in our models are not, in general, ultraluminous starbursts since they never experience exceptional star formation rates. In this case, Dickinson et al. (in preparation) and Pettini et al. (1997) argue that the likely correction is around a factor of $1.8 - 3$ at $z \sim 3$ for star formation rates inferred from 1500Å fluxes. These corrections are a factor of ~ 5 smaller than those advocated by Meurer et al. (1997). In Fig. 16, we illustrate the effect of the Pettini et al. correction at high redshift by multiplying the points of Madau et al. (1996) by a factor of 3 (open squares). The correction appropriate to the lower redshift points is also uncertain and we do not attempt to illustrate it in Fig. 16. It is likely to be smaller than at high redshift since the star formation rates are derived from longer wavelength data.

A related observational constraint on the evolution of the galaxy population comes from observations of neutral hydrogen at high redshift using quasar absorption lines. Fig. 17 compares the evolution of the cold gas fraction in our models with estimates by Storrie-Lombardi et al. (1996), derived from the statistics of damped Lyman-alpha absorption lines. Whereas Kauffmann's (1996b) semi-analytic models agree quite well with these data, our own models agree only in the qualitative sense that the comoving cold gas density has a broad peak at a redshift $z = 2$–3. Our models predict consistently more cold gas than is inferred from the observations. On the other hand, the observational results may underestimate the total cold gas density in galaxies because (i) they only include atomic hydrogen at column densities $N_H > 2 \times 10^{20} \mathrm{cm}^{-2}$, and do not include ionized or molecular gas at all; and (ii) dust obscuration may cause some absorption systems to be missed. Regarding (i), all the gas in our model galaxies at $T \lesssim 10^4 K$ is counted as "cold"; the correction for ionized gas and for low column-density HI ($N_H < 2 \times 10^{20} \mathrm{cm}^{-2}$) is probably not large, but the correction for molecular hydrogen might be significant. Regarding (ii), the chemical evolution models of Pei & Fall (1995) suggest that because of dust obscuration, the true neutral hydrogen density is 2-3 times higher than the "directly measured" value, moving the observational points in Fig. 17 much closer to the theoretical curves. The dotted-line set of errorbars in Fig. 17(a) show plausible corrections for these effects, using the output from one of the models of Pei & Fall (1995), following Figure 2 of Storrie-Lombardi et al. (1996).
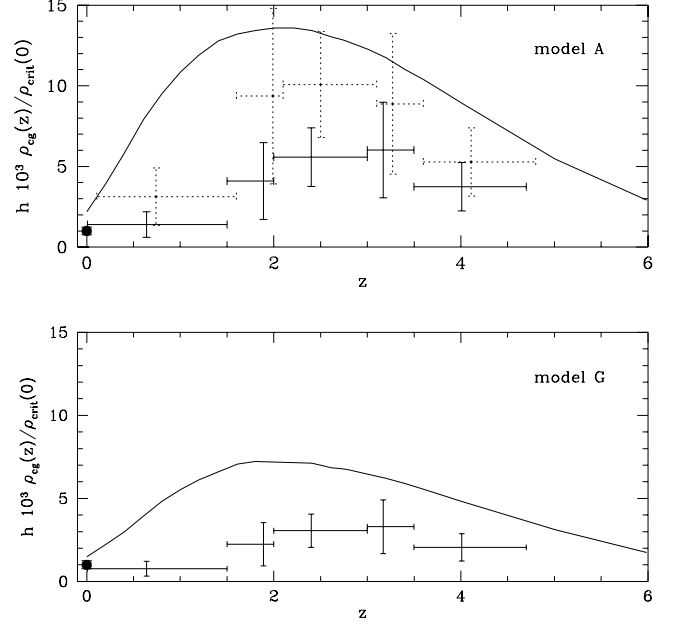
FIG. 17 The total comoving density of cold gas, ρ_{cg}, in units of the present critical density. The curve in the upper panel shows the evolution of ρ_{cg} with redshift in model A. The dependence of ρ_{cg} with redshift in models B and C which differ from A only in the choice of IMF, are identical to that in A. The curve in the lower panel shows results for model G. The data points are observational estimates, based on damped Lyman-alpha absorption lines from Storrie-Lombardi et al. (1996). We have applied an approximate scaling to their $\Omega = 1$ estimates to derive the corresponding values for the flat low-Ω model G. The data point at $z = 0$ is based on the HI luminosity function of nearby galaxies derived from 21cm observations. The dotted-line errorbars in the upper panel show the corrections to the data suggested by Storrie-Lombardi et al. to account for the effects of incompleteness and of dust obscuration, using a model from Pei & Fall (1995). We have retained the same fractional errors on the 'corrected' data points.
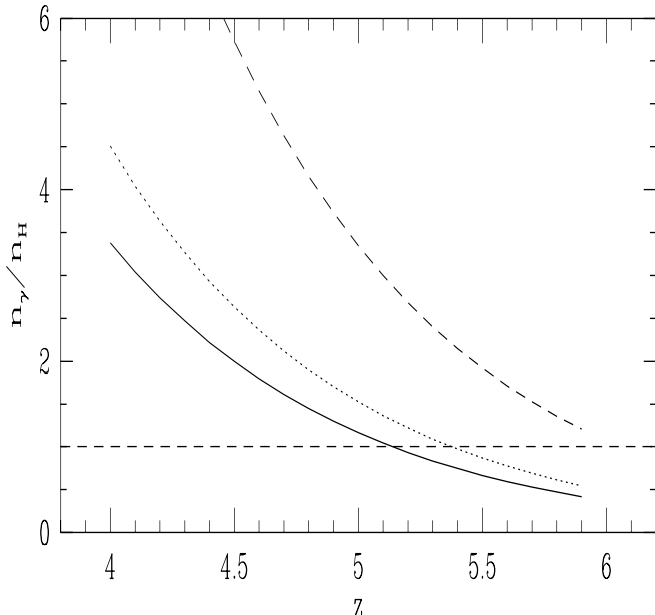
FIG. 18 The ratio of the number density n_γ of ionizing photons produced per comoving volume to the number density n_H of hydrogen atoms. At the redshift at which $n_\gamma/n_H = 1$, just enough ionizing photons have been produced to ionize every hydrogen atom exactly once. The solid line is for model A, the dotted for model G and the dashed for model C.

An interesting issue is whether massive stars in young galaxies can, on their own, produce enough ionizing photons ($\lambda < 912$Å) to re-ionize the IGM by $z = 5$. (Additional ionizing photons are produced by quasars, and possibly by pregalactic stars formed at high redshift via molecular hydrogen cooling, e.g. Tegmark et al. 1997). A very simple criterion for establishing if re-ionization is possible by redshift z is based on the ratio n_γ/n_H, where n_γ is the total number of ionizing photons produced per comoving volume up to redshift z, and n_H is the total comoving density of hydrogen atoms. When $n_\gamma/n_H = 1$, just enough ionizing photons are produced to ionize each hydrogen atom exactly once. This criterion neglects absorption of photons within the emitting galaxies, recombination of hydrogen in the IGM, and depletion of the IGM by collapse of gas into dark halos. In particular, the fraction f_{esc} of ionizing photons that escape from a galaxy may be quite low: Dove & Shull (1994) estimate $f_{esc} \sim 10\%$ for our own galaxy, while Leitherer et al. (1995) estimate $\langle f_{esc} \rangle \lesssim 3\%$ from far-UV observations of nearby starburst galaxies. The photon number density, n_γ, is also sensitive to the form of the IMF above $10 M_\odot$. Fig. 18 shows the dependence of n_γ/n_H on redshift for models A, C and G.

6. DISCUSSION

We have used a semi-analytic model of galaxy formation to interpret recent data on galaxy formation and evolution within the context of hierarchical clustering theories, focussing primarily on the properties of the recently discovered population of Lyman-break galaxies at $z \simeq 3$. Our

modelling technique allows us to identify the role that this population plays within the general scheme of galaxy formation, and to relate these observations to other data at lower redshifts. Our models are quite general, but they inevitably require a number of assumptions and simplifications most of which, in fact, reflect our poor understanding of the processes of star formation and feedback. Within these limitations we attempt to represent the relevant physics using scaling laws that involve the smallest possible number of free parameters. Our modelling strategy is based on fixing these free parameters by requiring that the models should match a small subset of the local data, particularly the field B-band galaxy luminosity function. Thus specified, the models possess predictive power and can be tested against high redshift data.

The specific cold dark matter models that we have considered all share the feature that they reproduce the observed abundance of present day rich clusters of galaxies. This fixes the amplitude of primordial density fluctuations which determines the epoch at which structures on any mass scale form. Current large-scale structure data allow a range of values for the cosmological parameters Ω_0 and Λ_0. By way of illustration, we have explored in detail a critical density model and two low-density models, one open and the other flat. A second common feature of the models we have considered is that they all agree at some level with most data on the evolutionary properties of galaxies at relatively modest redshifts, $z \lesssim 1$, such as the evolution of the luminosity function (Baugh et al. 1996a), and the counts of galaxies as a function of magnitude, morphological type, and redshift (Cole et al. 1994, Baugh et al. 1996b, Frenk et al. 1996). Several interesting predictions of the models have been corroborated by subsequent data, including, for example, the redshift distribution of $B = 24$ counts (Frenk et al. 1997).

An important prediction of semi-analytic models which also predated the acquisition of the relevant data is the cosmic star formation history, first discussed by White & Frenk (1991) and calculated by Cole et al. (1994) and Heyl et al. (1995) for the specific models discussed here (c.f. Fig. 14). We showed in Section 5 that Madau's (1996) recent data agree well with these model predictions, although uncertainties remain in this comparison because of the unknown effects of dust obscuration and possible incompleteness in the observational samples at high redshifts. In particular, the possibility that a significant fraction of the total star formation may have been missed in recent surveys if it occured in dust enshrouded starbursts at very high redshift has been the subject of some recent debate. Such a population is not predicted in our models, although a certain amount of dust obscuration at high redshift can be accommodated and may even be required: our models, in fact, predict star formation rates which are somewhat higher than those inferred from the data uncorrected for dust obscuration (c.f. Fig. 16). The star formation rate in our models peaks around $z = 1 - 2$, but it never varies by more than an order of magnitude over the entire range $0 < z < 6$. In fact, the star formation rate at $z \simeq 5$ is almost identical to the star formation rate at the present day. Nevertheless, half of all the stars present today only formed since $z < 1$. The significance of the Lyman-break galaxies in the context of these models

lies in the fact that at the epoch when these galaxies are observed, the process of star formation is just beginning in earnest. Thus the Lyman-break galaxies are the first massive objects to sustain appreciable star formation and, in this sense, they signal the onset of galaxy formation.

The *distribution* of star formation rate at different redshifts provides even stronger constraints on models than the evolution of the integrated star formation rate. Our models match existing data quite well, and further observational measurements of this fundamental quantity are very important. In both models and observations, the quiescent star formation rates are relatively low even in the largest protogalaxies, with the majority of galaxies never forming stars at rates exceeding a few solar masses per year. The exception to this are galaxies that undergo a burst of star formation as a result of experiencing a major merger. However, predictions for the strength, duration and frequency of such bursts will require more detailed modelling that we have attempted so far.

In our models, the Lyman-break galaxies form from rare peaks in the density field at high redshift. As a result, we predict that their spatial distribution at $z \simeq 3$ should be strongly biased relative to the underlying mass, with a typical bias parameter, $\bar{b} \simeq 4$, and a comoving clustering length, $r_0 \simeq 4h^{-1}$Mpc. Generically, we expect the Lyman-break galaxies to be rotating disks, and a simple model for the origin of their angular momentum predicts typical half-light radii of $\simeq 0.5h^{-1}$kpc. The Lyman-break galaxies seen at $z \simeq 3$ evolve into the present day ordinary ellipticals and spirals that make up the bright end of the luminosity function. Their stars will typically be concentrated in the central regions of their descendants. These descendants are to be found preferentially in groups and clusters, reflecting their biased origin and strong clustering at high redshift.

The appearance of the first protogalaxies at $z \simeq 3.5$ and the late conversion of most of the gas into stars fit in well with the observation that the neutral hydrogen content of the universe, as determined from measurements of damped Lyman-alpha clouds, peaks at around $z = 3$ and declines thereafter (Storrie-Lombardi et al. 1996). The neutral hydrogen density in our models also exhibits this overall behaviour and agrees reasonably well with the data once corrections for incompleteness and a small amount of dust obscuration are included. Related semi-analytic models by Kauffmann (1996b) agree even better with these data. Our models are consistent with Madau's (1996) view that, with the discovery of Lyman-break galaxies, the bulk of the star formation (and the attendant metal production) in our universe has, in effect, been identified. Only a small fraction of the star formation activity remains to be detected during the "dark ages" prior to $z = 4$. Characterising such activity is, of course, of great importance for testing the general view that galaxies formed by hierarchical clustering. According to our models, the small percentage of stars that formed prior to the Lyman-break galaxy epoch produce enough radiation to make at least a significant contribution to the UV flux required photoionize the intergalactic medium by $z \simeq 5$.

Although a late epoch of galaxy formation in the standard CDM model was predicted long ago (Frenk et al. 1985, White & Frenk 1991), a surprising result of our analysis is that this is also true of the now popular low-density variants of this model. Indeed, the star formation histories of the $\Omega_0 = 1$ model and the flat $\Omega_0 = 0.3$ model are remarkably similar. This is largely coincidental: the detailed star formation histories depend not only on the shape of the power spectrum, but also on its normalisation and on the way in which star formation and feedback are implemented in our galaxy formation models. The main conclusion of our analysis is that, regardless of the exact values of the cosmological parameters, CDM models that approximately reproduce the abundance of Lyman-break galaxies, require massive galaxy formation to begin around $z \simeq 3.5$.

In summary, we have argued in this paper that the main ingredients of a consistent picture of galaxy formation may now be in place. The key observation that has unlocked this paradigm is the discovery of a large population of star-forming galaxies at $z \simeq 3$ which signal the onset of the epoch of galaxy formation that extends well into the present day. At this time, data and theoretical modelling paint only a broad brush picture of how galaxy formation may have occurred. Fortunately, if this emerging picture is correct, the details should also be accessible to current observational and modelling capabilities.

REFERENCES

Abraham, R.G., Tanvir, N.R., Santiago, B.X., Ellis, R.S., Glazebrook, K., Van den Bergh, S., 1996 MNRAS, 279, L47

Baron, E., White, S.D.M., 1987, Astroph. J., 322, 585

Baugh, C.M., Efstathiou, G., 1993, MNRAS, 265, 145

Baugh, C.M., Cole, S., Frenk, C.S., 1996a, MNRAS, 282, L27

Baugh, C.M., Cole, S., Frenk, C.S., 1996b, MNRAS, 283, 1361

Bennet, C.L. et al. 1996, Astroph. J., 464 L1

Bond, J.R., Cole, S., Efstathiou, G., Kaiser, N., 1991, Astroph. J., 379, 440

Bower, R.G., 1991, MNRAS, 248, 332

Brainerd, T.G., Smail, I., Mould, J. 1995, MNRAS, 275, 781

Bruzual, G., Charlot, S., 1993, Astroph. J., 405, 538

Charlot, S., Worthey, G., Bressan, A., 1996, Astroph. J., 457, 625

Cole, S., 1991, Astroph. J., 367, 45

Cole, S., Kaiser, N., 1988, MNRAS, 233, 637

Cole, S., Aragón-Salamanca, A., Frenk, C.S., Navarro, J.F., Zepf, S.E., 1994, MNRAS, 271, 781

Cole, S., Weinberg, D.H., Frenk, C.S., Ratra, B., 1997, MNRAS, 289, 37

Connolly, A.J., Szalay, A.S., Dickinson, M., SubbaRao, M.U., Brunner, R.J. 1997, Astroph. J., 486, L11

Copi, C.J., Schramm, D.N., Turner, M.S., 1996, Nucl. Phys. B., S51B, 66.

Cowie, L.L., Songaila, A., Hu, E.M., Cohen, J.G., 1996, Astroph. J., 112, 839

Dove, J.B, Shull, J.M., 1994, Astroph. J., 430, 222

Dressler, A., Oemler, A., Sparks, W.B., Lucas, R.A., 1994, Astroph. J., 435, L23

Driver, S.P., Windhorst, R.A., Griffiths, R.E., 1995, Astroph. J., 453, 48

Eggen, O.J., Lynden-Bell, D., Sandage, A.R., 1962, Astroph. J., 136, 748

Eke, V.R., Cole, S., Frenk, C.S., 1996, MNRAS, 282, 263

Ellis, R.S., Colless, M., Broadhurst, T., Heyl, J., Glazebrook, K., 1996, MNRAS, 280, 235

Frenk, C.S., Baugh, C.M., Cole, S., 1996, IAU Symposia 171, 247

Frenk, C.S., Baugh, C.M., Cole, S., Lacey, C.G., 1997 to appear in Dark Matter and Visible Matter in Galaxies, eds. M. Persic & P. Salucci.

Gallego, J., Zamorano, J., Aragón-Salamanca, A., Rego, M., 1995, Astroph. J., 455, L1

Giavalisco, M., Steidel, C.C., Macchetto, F.D., 1996, Astroph. J., 470, 189

Glazebrook, K., Ellis, R., Santiago, B., Griffiths, R., 1995a, MNRAS, 275, L19

Glazebrook, K., Ellis, R., Colless, M., Broadhurst, T., Allington-Smith, J., Tanvir, N., 1995b, MNRAS, 273, 157

Guiderdoni, B., Hivon, E. Bouchet, F. R., Maffei, B. 1997a, MNRAS, in press.

Guiderdoni, B., Bouchet, F. R., Puget, J. L., Lagache, G, & Hivon, E. 1997b, Nature, in press.

Heyl, J.S., Cole, S., Frenk, C.S., Navarro, J.F., 1995, MNRAS, 274, 755

Kashlinsky, A., Mather, J.C., Odenwald, S., 1996, Astroph. J., 437 L9.

Kauffmann, G., 1995, MNRAS, 274, 161

Kauffmann, G., 1996a, MNRAS, 281, 475

Kauffmann, G., 1996b, MNRAS, 281, 487

Kauffmann, G., White, S.D.M., Guiderdoni, B., 1993, MNRAS, 264, 201

Kauffmann, G., Guiderdoni, B., White, S.D.M., 1994, MNRAS, 267, 981

Kauffmann, G., Charlot, S., White, S.D.M., 1996 MNRAS, 283, L117

Lacey, C.G., Cole, S. 1993 MNRAS, 262, 627

Lacey, C.G., Guiderdoni, B., Rocca-Volmerange, B., Silk, J., 1993, Astroph. J., 402, 15

Lacey, C.G., Silk, J., 1991 Astroph. J., 381,14

Lanzetta, K.M., Wolfe, A.M., Turnshek D.A., 1995, Astroph. J., 440, 435

Leitherer, C., Ferguson, H.C., Heckman, T.M., Lowenthal, J.D., 1995, Astroph. J., 454, L19

Liddle, A. R., Lyth, D. H., Viana, P. T. P., White, M., 1996, MNRAS, 282, 281

Lilly, S.J., Tresse, L., Hammer, F., Crampton, D., LeFevre, O, 1995, Astroph. J., 455, 108

Lilly, S.J., LeFevre, O, Hammer, F., Crampton, D., 1996, Astroph. J., 460, L1

Limber, D. N., 1954, Astroph. J., 119, 655

Loveday, J., Peterson, B.A., Efstathiou, G., Maddox, S.J., 1992, Astroph. J., 390, 338

Lowenthal, J. D., Koo, D. C., Guzman, R., Gallego, J., Phillips, A. C., Faber, S. M., Vogt, N. P., Illingworth, G. D., Gronwall, C., 1997, Astroph. J., 481, 673

Lu, L.M., Sargent, W.L.W., Womble, D.S., Takadahidai, M., 1996, Astroph. J., 472, 509

Marzke, R.O., Huchra, J.P., Geller, M.J., 1994, Astroph. J., 428, 43

Madau, P., 1995, Astroph. J., 441, 18

Madau, P., 1996, preprint astro-ph/9612157

Madau, P., Ferguson, H.C, Dickinson, M., Giavalisco, M., Steidel, C.C., Fruchter, A., 1996, MNRAS, 283, 1388

Madau, P., Pozzetti, L., Dickinson, M., 1997, submitted to Astroph. J., astro-ph/9708220

Meurer, G.R., Heckman, T.M., Lehnert, M.D., Leitherer, C., Lowenthal, J. 1997, Astron. J., , 114, 54

Miller, G.E., Scalo, J.M., 1979, Astroph. J. Suppl., 41, 513

Mo, H.J., Fukugita, M., 1996, Astroph. J., 467, L9

Mo, H.J., Jing, Y.P., White, S.D.M., 1996, MNRAS, 282, 1096

Mo, H.J., White, S.D.M., 1996, MNRAS, 282, 347

Navarro, J.F., Frenk, C.S., White, S.D.M., 1996, Astroph. J., 462, 563

Odewahn, S.C., Windhorst, R.A., Driver, S.P., Keel, W.C., 1996, Astroph. J., 472, L13

Pascarelle, S.M., Windhorst, R.A., Keel, W.C., Odewahn, S.C. 1996, Nature, 383, 45

Peacock, J.A., Dodds, S.J., 1996, MNRAS, 280, L19

Peebles, P.J.E., 1980, Large Scale Structure in the Universe Princeton.

Pei, Y.C., Fall, S.M, 1995, Astroph. J., 154, 69

Pettini, M., Smith, L.J., King, D.L., Hunstead,R.W., 1997, Astroph. J., 486, 665

Pettini, M., Steidel, C.C., Adelberger, K.L., Kellogg, M., Dickinson, M., Giavalisco, M., 1997, To appear in 'ORIGINS', ed. J.M. Shull, C.E. Woodward, and H. Thronson, (ASP Conference Series) (astro-ph/9708117)

Press, W.H., Schechter, P.L., 1974, Astroph. J., 187, 425

Puget, J.L., Abergel, A., Bernard, J.P., Boulanger, F., Burton, W.B., Desert, F.X., Hartmann, D., 1996, Astron. Astrop., 308, L5

Sawicki, M.J., Lin, H., Yee, H.K.C. 1997, Astron. J., 113, 1

Salpeter, E.E., 1955, Astroph. J., 121, 61

Scalo, J.M., 1986, Fundamentals of Cosmic Physics, 11, 1

Smail, I., Dressler, A., Kneib, J.P., Ellis, R.S., Couch, W.J., Sharples, R.M., Oemler, A., 1996, Astroph. J., , 469, 508.

Smail, I., Dressler, A., Couch, W.J., Ellis, R.S., Oemler, A., Butcher, H., Sharples, R.M., 1997, Astroph. J. Suppl., 110, 213

Steidel, C.C., Hamilton, D., 1992, Astron. J., 104, 941

Steidel, C.C., Hamilton, D., 1993, Astron. J., 105, 2017

Steidel, C.C., Pettini, M., Hamilton, D., 1995, Astron. J., 110, 2519

Steidel, C.C., Giavalisco, M., Pettini, M., Dickinson, M., Adelberger, K.L., 1996a, Astroph. J., 462, L17 (S96).

Steidel, C.C., Giavalisco, M., Dickinson, M., Adelberger, K.L., 1996b, Astron. J., 112, 352

Storrie-Lombardi, L.J., McMahon, R.G., Irwin, M.J., 1996, MNRAS, 283, L79

Tegmark, M., Silk, J., Rees, M.J., Blanchard, A., Abel, T., Palla, F., 1997, Astroph. J., 474,1

Treyer, M.A., Ellis, R.S., Milliard, B., Donas, J., 1997, to appear in "The Ultraviolet Universe at Low and High Redshift: Probing the Progress of Galaxy Evolution", AIP press

Tytler, D., Fan, X.M., Burles, S., 1996, Nature, 381, 207

Viana, P.T.P., Liddle, A.R., 1996, MNRAS, 281, 323

White, S.D.M., Efstathiou, G., Frenk, C.S., 1993, MNRAS, 262, 1023

White, S.D.M., Frenk, C.S., 1991, Astroph. J., 379, 52

White, S.D.M., Rees, M.J., 1978, MNRAS, 183, 341.

Williams, R.E., et al. 1996, Astron. J., 112, 1335.

Wolfe A.M., Lanzetta K.M., Foltz C.B., Chaffee, F.H., 1995, Astroph. J., 454, 698